fluids

MDPI

Article

Multi-Scenario Resistance Optimisation of an Indonesian Pioneer Vessel Through Response Surface Method

Muhammad Iqbal *, Andi Trimulyono *, Ammarunissa Noor Asiyah Raihannanda, Azka Maulana Widestra, Berlian Arswendo Adietya and Ahmad Firdhaus

Department of Naval Architecture, Diponegoro University, Semarang 50275, Indonesia; ammarunissa@students.undip.ac.id (A.N.A.R.); amwidestra@students.undip.ac.id (A.M.W.); berlianarswendoadiet@lecturer.undip.ac.id (B.A.A.); afirdhaus@lecturer.undip.ac.id (A.F.)

* Correspondence: muhammadiqbal@lecturer.undip.ac.id (M.I.); anditrimulyono@lecturer.undip.ac.id (A.T.)

Abstract

Improving ship hydrodynamic efficiency is an important strategy for reducing fuel consumption and operational costs. This study investigates the optimisation of ship resistance through a combined approach involving hull form modification and operational trim adjustment. The research focuses on a pioneer vessel model, where hydrodynamic performance is analysed using Computational Fluid Dynamics (CFD) simulations coupled with Central Composite Design (CCD) and the Response Surface Methodology (RSM). Prior to the optimisation analysis, the CFD model was verified through a grid convergence study and validated against towing tank experimental data, showing good agreement. The optimisation was conducted through three scenarios: hull form optimisation, trim optimisation, and integrated optimisation, which combined both strategies. The statistical analysis revealed that longitudinal parameters play a dominant role in resistance reduction. In particular, the longitudinal centre of buoyancy (LCB) was identified as the most influential parameter in hull form optimisation, while the longitudinal centre of gravity (LCG) was the dominant parameter in trim optimisation. The results show that hull form optimisation alone reduced resistance by approximately 6%, while trim optimisation achieved a reduction of about 4%. The integrated optimisation strategy produced the greatest improvement, resulting in resistance reduction of nearly 10% compared with the baseline configuration. The findings highlight the importance of integrating design-stage optimisation and operational optimisation in improving ship hydrodynamic performance. However, the optimisation was limited to calm-water conditions.

Keywords: ship resistance; hull form optimisation; trim optimisation; computational fluid dynamics (CFD); response surface methodology (RSM); central composite design (CCD)

Check for updates

Academic Editor: Giuliano De Stefano

Received: 10 April 2026
Revised: 12 May 2026
Accepted: 13 May 2026
Published: 18 May 2026

Copyright: © 2026 by the authors. Licensee MDPI, Basel, Switzerland. This article is an open access article distributed under the terms and conditions of the Creative Commons Attribution (CC BY) license.

1. Introduction

Maritime transportation plays a crucial role in supporting economic connectivity and logistics distribution in archipelagic countries. In nations with a dispersed island geography such as Indonesia, pioneer vessels function as essential feeder ships that connect remote regions with major trade hubs, facilitating both passenger mobility and the distribution of goods.

In international maritime terminology, the term pioneer vessel (*kapal perintis*) is not commonly used as a formal ship classification. In the Indonesian context, however, *kapal perintis* refers to government-subsidised passenger–cargo vessels that provide essential

maritime transport services to remote, underdeveloped, outermost, and border regions where commercial shipping operations are economically unfeasible. These vessels operate under a public service obligation (PSO) scheme to ensure the distribution of basic necessities, support population mobility, and maintain socio-economic connectivity among isolated island communities. Therefore, within this study, the term pioneer vessel is used to denote such subsidised inter-island service vessels operating in remote areas of the Indonesian archipelago.

However, the operational sustainability of such vessels is strongly influenced by fuel consumption, which constitutes a substantial portion of the total operating cost. Previous studies report that fuel expenses can account for approximately 50–60% of a vessel's overall operational cost, highlighting the importance of improving ship energy efficiency through hydrodynamic optimisation [1], such as hull form optimisation [2,3], trim optimisation [4], and addressing hull fouling [5].

From a hydrodynamic perspective, ship resistance represents the primary component influencing propulsion power and fuel consumption. When a ship advances in water, it experiences several resistance components, including frictional resistance, viscous pressure resistance, and wave-making resistance. Among these, wave-making resistance becomes particularly significant at moderate operating speeds, characterised by specific ranges of the Froude number. At low Froude numbers, wave-making resistance is minimal. Computational Fluid Dynamics (CFD) and towing tank experiments consistently show that wave-making resistance increases quadratically with Froude number in many cases [6].

Medium-sized displacement vessels, including feeder ships and pioneer vessels operating in archipelagic regions, exhibit hydrodynamic characteristics that differ from those of high-speed craft or large ocean-going cargo ships. These ships can be categorised as 'low-to-medium-speed displacement vessels', which typically operate within moderate ranges of the Froude number, where both viscous resistance and wave-making resistance contribute significantly to the total resistance. In particular, the interaction between bow and stern wave systems becomes increasingly important as vessel speed approaches the critical Froude number region, where wave-making resistance increases rapidly. Understanding these hydrodynamic behaviours is therefore essential for improving the performance of feeder vessels operating in calm-water conditions.

The primary difficulty lies in the nonlinear transition as the speed increases. This involves intricate wave interactions, flow separation at the round bilge, and the coexistence of steady and unsteady movements [7]. To reduce the wave resistance at higher speeds, Çelik and Danışman [8] used a hull vane. The effective power reduced by 11.41%, propulsive efficiency increased by 2.1, and the wave resistance component was reduced. When sailing at lower speeds, the total resistance is dominated by viscous resistance rather than wave resistance. To reduce this type of resistance, air lubrication can be used. Krishnan et al. [9] used Air Layer Drag Reduction (ALDR) for KVLCC2. Meanwhile, Park and Lee [10] used the same method for a tanker ship with multiple injection schemes. Drag reduction of up to 18% was achieved close to the design speed.

On the other hand, total resistance still can be reduced without additional devices by optimising the hull form. Zhang et al. [11] used semi-parametric deformation techniques, including delta shift (for bow shape), freeform deformation (for bow and stern width), and Lackenby transformation (for hull form), to optimise the hull form, achieving a reduction of about 5.43% in total resistance compared to the original design at the same design speed (22 knots). Modifying geometric parameters such as the longitudinal centre of buoyancy (LCB), the prismatic coefficient, and the sectional area distribution can significantly influence the flow pattern around the hull and thus alter the resistance characteristics [12,13]. Computational and experimental studies have shown that carefully designed hull modifications

can lead to measurable reductions in total resistance and improved energy efficiency of ships [2]. In real-world operations, ships sail at different speeds depending on mission requirements, sea states, and operational scenarios. Liu et al. [14] invested significant effort into hull form optimisation by including multiple speeds as variables. Their optimised hull forms reduced resistance by 2.95–5.51% across the six tested speeds, with improvements being most notable at mid-range speeds (Fr = 0.28–0.30).

Despite these advancements, hull geometry optimisation is generally most effective during the early design stage of a vessel. Implementing geometric modifications on ships that are already in service is often impractical due to structural and economic constraints. Consequently, operational optimisation strategies have attracted increasing attention as an alternative approach to improving ship efficiency without altering the physical structure of the hull. One of the most influential operational parameters is trim, as investigated by [15–17]. Variations in trim alter the wetted surface area, pressure distribution, and wave-making characteristics, thus directly impacting total resistance [18]. Furthermore, trim significantly influences seakeeping and added resistance, as evidenced by studies on the KCS model [19]; additionally, when applied to the stern, trim can enhance intact stability by 0.5% to 5.4% in tankers, container ships, and bulk carriers [20].

In addition to operational optimisations, modern hydrodynamic analysis increasingly relies on Computational Fluid Dynamics (CFD) to predict ship resistance and flow characteristics with high fidelity. CFD simulations based on Reynolds-averaged Navier–Stokes equations have widely been applied to investigate the resistance and propulsion performance of various ship types under controlled numerical conditions. These numerical tools enable detailed analysis of flow fields, wave patterns, and pressure distributions around the hull while reducing the cost and time associated with extensive towing tank experiments.

Statistical optimisation techniques, such as the Response Surface Methodology (RSM), are increasingly being adopted within ship design studies. The RSM facilitates the development of surrogate models that approximate the relationship between design variables and hydrodynamic responses. This allows for an efficient exploration of the design space and the identification of optimal configurations using significantly fewer simulations [21–24] than the machine-learning-based optimisation conducted by [11], which required 200 data points.

Although extensive research has been conducted on hull form optimisation and trim optimisation individually, relatively few studies have examined the combined influence of these two strategies within a unified optimisation framework. Most existing studies focus either on the geometric modification of new ship designs or on operational adjustments of existing vessels, rarely comparing the effectiveness of these approaches directly.

Furthermore, research specifically addressing medium-sized displacement feeder vessels such as pioneer ships remains limited, despite their critical role in regional maritime transportation networks. As a result, there is still a lack of comprehensive studies that evaluate how geometric and operational optimisation strategies interact and contribute to overall resistance reduction.

To address this gap, the present study proposes a multi-scenario optimisation framework that integrates hull geometry modification and trim optimisation using CFD and statistical modelling techniques. By evaluating three optimisation scenarios, namely hull form optimisation, trim optimisation, and an integrated hybrid approach, this study aims to provide deeper insights into the relative effectiveness of design-based and operational-based strategies for reducing the resistance of pioneer vessels.

2. Method

2.1. Research Design

Figure 1 shows the flowchart of the research. Prior to undertaking the optimisation study, the subject vessel and the corresponding simulation conditions were defined based on available experimental test data. These experimental results provided the necessary reference for establishing the numerical model and ensuring that the simulation setup realistically represented the physical conditions of the towing experiments.

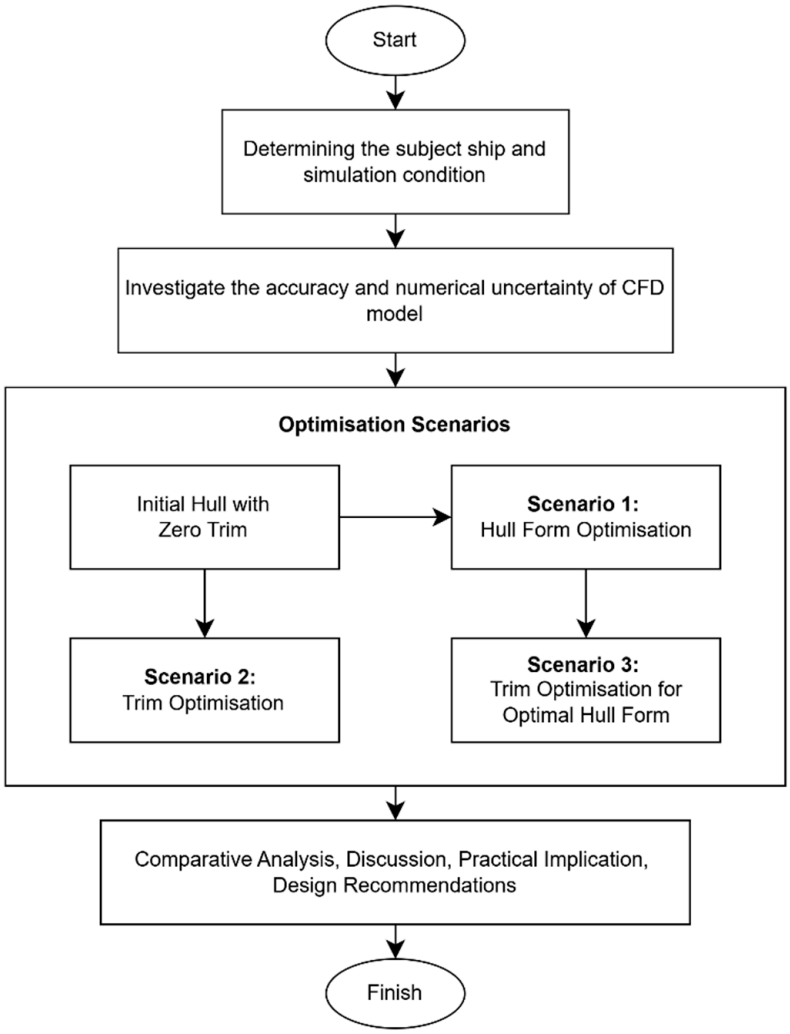


Figure 1. Research flowchart.

Following this, a series of Computational Fluid Dynamics (CFD) simulations were carried out to verify the accuracy of the numerical model. This stage included validation against the experimental measurements and an assessment of numerical uncertainty through a grid convergence study. The purpose of this procedure was to ensure that the predicted hydrodynamic resistance was not significantly influenced by discretisation errors and that the numerical model could produce reliable results.

After the numerical model had been verified, three optimisation scenarios were assessed. All scenarios were based on the lowest speed, which is 1.455 m/s in the scale model (Fr = 0.257). For each scenario, a series of simulation cases were generated using Central Composite Design in order to systematically explore the influence of the selected design variables. The results obtained from these simulations were then analysed using the Response Surface Methodology to develop regression models that describe the relationship

between the design variables and the resulting ship resistance. These models enable the response behaviour to be represented through second-order polynomial functions. Finally, the optimal configuration was identified through an analysis of the response surfaces derived from the regression models. By examining these surfaces, the combination of parameters that yields the minimum total resistance of the vessel was determined.

The results obtained from these optimisation studies were subsequently analysed and discussed in detail to identify the configuration that produced the minimum hydrodynamic resistance. The main findings of this study are summarised in the Conclusion, highlighting the effectiveness of each optimisation strategy and their implications for improving ship performance.

2.2. Optimisation Scenarios

Scenario 1—Hull Form Optimisation

The first scenario involved hull form optimisation through a parametric transformation technique. Using this approach, the hull geometry was modified using the Lackenby transformation, which enables systematic adjustments to the longitudinal distribution of the sectional area curve while maintaining the vessel's length (L), draught (T), and displacement (Δ), with the sole exception of the ship's beam (B), which is adjusted and block coefficient (cb) is targetted. Two design variables were considered in this scenario: the longitudinal centre of buoyancy (LCB) and the block coefficient (Cb). Altering these parameters directly redistributes the sectional area curve (SAC) of the hull, thus changing its physical underwater form by shifting x by a distance δx, as shown in Figure 2. These parameters were varied according to the combinations specified in the Central Composite Design matrix. For each generated hull configuration, a CFD simulation was conducted to determine the corresponding total resistance, allowing the influence of the geometric modifications to be quantified.

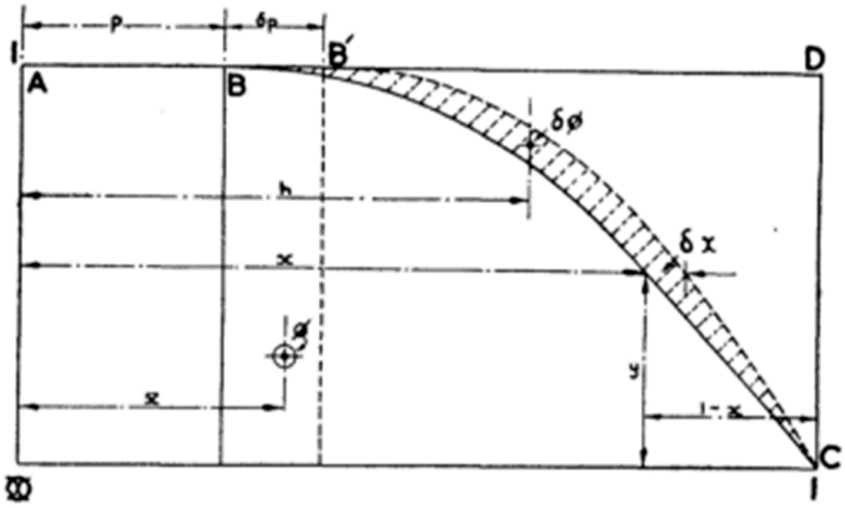


Figure 2. Forebody of CSA deformation by Lackenby [25] taken from Kramer [26].

Scenario 2—Trim Optimisation for Initial Hull

The second scenario comprised trim optimisation while retaining the original hull geometry of the vessel. In this case, variations in trim were introduced by adjusting the longitudinal and vertical positions of the centre of gravity, represented by LCG and VCG, respectively. The initial position of the longitudinal centre of gravity was assumed to coincide with the longitudinal centre of buoyancy (LCB), while the initial vertical centre of gravity (VCG) was taken as 75% of the ship's KM.

Altering these parameters modifies the trim angle of the vessel, which in turn affects the wetted surface area and the pressure distribution along the hull. Theoretically, any shift in LCG relative to LCB generates a longitudinal trimming moment, $M_{trim} = \Delta \times (LCG - LCB)$, forcing the vessel to rotate until a new equilibrium is reached, where G and B are vertically aligned. Meanwhile, a shift in VCG results in a change in the longitudinal metacentric height, $GM_L = KB + BM_L - KG$, which changes the stiffness of the vessel's response to trimming moments. For each trim configuration specified in the Central Composite Design matrix, a CFD simulation was carried out to evaluate the resulting resistance.

Scenario 3—Integrated Optimisation (Trim Optimisation for Optimal Hull)

The third scenario integrated the outcomes of the two preceding optimisation stages. The hull form identified as optimal in Scenario 1 was adopted as the new baseline geometry. Using this modified hull form, a subsequent trim optimisation was conducted to determine the most favourable operational condition. By combining hull-form modification with trim adjustment, this approach seeks to identify the overall configuration that yields the lowest hydrodynamic resistance. Finally, the results obtained from all three scenarios were compared with those of the original vessel configuration. This comparison allows the effectiveness of each optimisation strategy to be evaluated and highlights the relative contribution of hull-form optimisation and trim optimisation to the overall resistance reduction.

2.3. Research Object and Experimental Data

The object of this study was a pioneer vessel operating in Indonesian waters, serving as a representative example of medium-displacement feeder ships commonly used for regional transportation. The hydrodynamic characteristics of the vessel were investigated. Experimental resistance tests were conducted using a scaled model in a towing tank facility. The model scale employed in the experiment was 1:18, and the principal dimensions of the model are summarised in Table 1.

Table 1. Principal dimensions of the model vessel (scale 1:18).

Dimensions	Value	
	Full Scale	**Model Scale (1:18)**
Length Overall, LOA (m)	63.80	3.544
Length on Waterline (m)	57.00	3.275
Breadth moulded, B (m)	11.60	0.8
Depth moulded, D (m)	4.5	0.25
Loaded Draft T (m)	2.90	0.161
Volume Displacement Δ (m^3)	1134.63	0.194
Block coefficient, C_b (-)	0.572	0.572
Mid-boat section coefficient, Cm (-)	0.945	0.945
Wetted surface area, Aw (m^2)	666.99	2.059

During the towing tank experiment, the model was tested under calm-water conditions with a towing speed of 1.455 m/s to 2.061 m/s, representing 12 to 17 knots at full scale or from Fr 0.26 to 0.36. The experimental measurements obtained from these tests were used as reference data for validating the numerical simulations performed in the present study. The experimental resistance data provide an essential benchmark for evaluating the

accuracy of the computational model and ensuring that the numerical results can reliably represent the hydrodynamic behaviour of the vessel.

2.4. Numerical Simulation Setup

The simulations were conducted by solving the Reynolds-averaged Navier–Stokes (RANS) equations coupled with a free-surface modelling approach.

2.4.1. Physical Models

The numerical simulation was performed by solving the Reynolds-averaged Navier–Stokes (RANS) equations to describe the viscous flow around the vessel. Turbulence was accounted for using the k-ε turbulence model, a commonly adopted approach in ship hydrodynamics because of its robustness and its ability to represent boundary layer behaviour at higher y^+ values. The interface between water and air was represented using the Volume of Fluid (VOF) technique, which tracks the volume fraction of each phase within the computational cells. This method enables simulation to capture wave formation and the deformation of the free surface generated by the moving hull. For the numerical solution, the governing equations were discretised spatially using a second-order convection scheme to improve solution accuracy. Time integration was carried out using a first-order implicit formulation, providing numerical stability during the simulation process.

2.4.2. Computational Domain and Boundary Conditions

To represent the experimental towing conditions numerically, a virtual towing tank was created around the ship model. The size of the computational domain was selected to be sufficiently large to minimise the influence of boundary effects on the flow solution. The inlet boundary was placed at a distance of one ship length (1 L) upstream of the bow, while the outlet boundary was extended to two ship lengths (2 L) downstream of the stern. In the transverse and vertical directions, the side and bottom boundaries were located at a distance of 1 L from the vessel centreline and below the free surface, respectively. Meanwhile, the upper boundary of the domain was positioned at 0.4 L above the free surface.

Boundary conditions were applied throughout the computational domain to reproduce the physical flow conditions. A velocity inlet condition was specified at the upstream, side, bottom, and top boundaries to impose the incoming flow corresponding to the towing speed used in the experiments. The downstream boundary was defined as a pressure outlet, enabling the fluid to leave the domain without artificial restriction. The ship hull was modelled as a no-slip wall to represent viscous effects at the surface, while the centreline plane of the domain was treated as a symmetry boundary to reduce computational cost.

2.4.3. Mesh Generation

The computational domain was discretised using an automatically generated mesh (Figure 3), complemented by prism layers applied along the hull surface to resolve the boundary layer flow. Three prism layers, calculated based on [27], were implemented with a stretching factor of 1.2, resulting in a target y^+ value of approximately 100. The total thickness of the prism layer region surrounding the hull was 0.0112891 m. Additional mesh refinement was introduced in the Kelvin wake region to ensure accurate resolution of the wave pattern. The transverse wavelength (λ) of the Kelvin wake was estimated using Equation (1), where k denotes the wave number, g denotes the gravitational acceleration, and V represents the ship speed. Based on this prediction, a refinement zone was defined behind the vessel, extending up to one ship length (1 L) downstream and bounded by an ingress angle of 20°.

Within this region, the mesh density was increased to provide 24 cells per transverse wavelength, resulting in a size of 0.0564 m, which determined the corresponding cell

length and width. This was then used as the base size. The vertical cell dimensions were further constrained, with the cell height set to one-eighth of the cell length in the streamwise (x) direction [3,27]. Close to the free surface, the mesh spacing was relaxed, with cell dimensions increasing by a factor of two relative to those used in the Kelvin wake refinement zone. The mesh setup in this study is shown in Table 2.

$$\lambda = \frac{2\pi}{k} = \frac{2\pi}{(g/V^2)} \tag{1}$$

Table 2. Mesh setup.

Default Control	Background	Overset
Base size	0.0564 m	
Target surface size	50%	50%
Minimum surf. Size	50%	50%
Volume growth rate	Fast	Slow
Max cell size	1600%	50%
Number of prism layers	-	3
Prism layer stretching	-	1.2
Prism layer tot. thickness	-	0.01129 m
Custom Control for Background		
Background surface		
- Target and min surface size	1600%	
Kelvin volume grid size		
- X ($\lambda/24$)	100%	
- Y ($\lambda/24$)	100%	
- Z (X/8)	12.50%	
Free surface background volume grid size		
- X ($\lambda/24 \times 2$)	200%	
- Y ($\lambda/24 \times 2$)	200%	
- Z ($X/8 \times 2$)	25%	
Overlap volume grid size		
- X	50%	
- Y	50%	
- Z	50%	
Custom Control Overset		
Ship surface		
- Target and min surface size	12.5%	
Free surface overset volume grid size		
- Z (X/8)	12.5%	

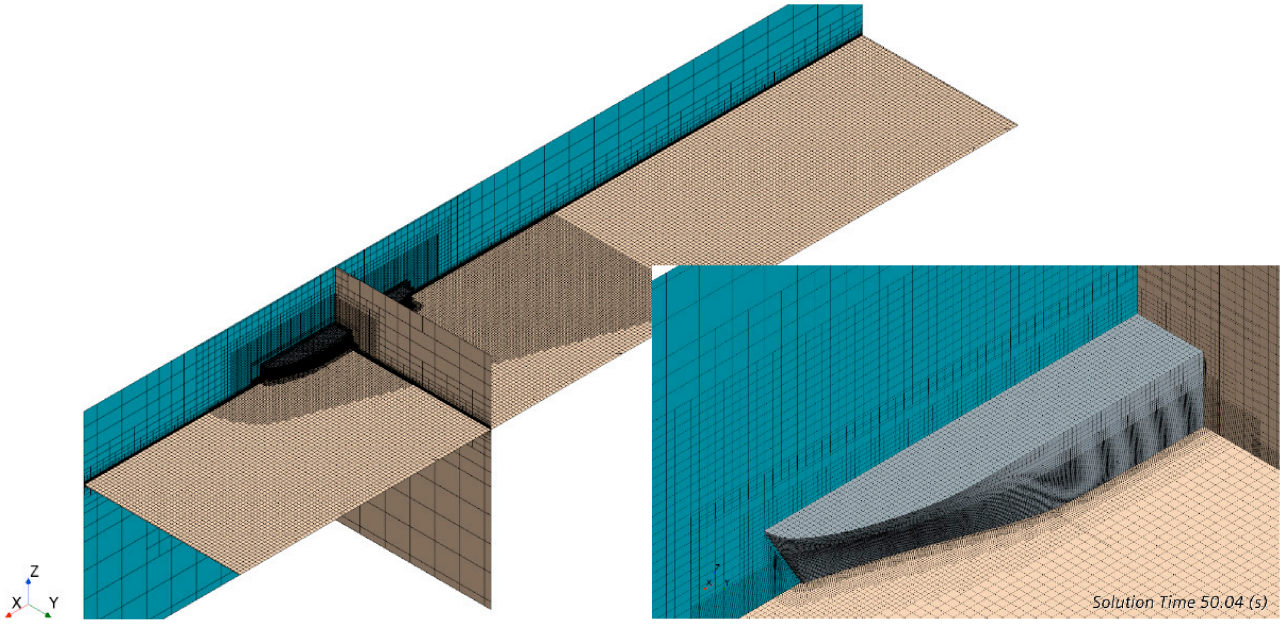


Figure 3. Resulting mesh.

2.4.4. Time Step

The time step used in the calm-water resistance simulations was determined in accordance with the recommendation of the International Towing Tank Conference [28]. The formulation, presented in Equation (2), relates the time step to the ship length (L) in metres and the ship speed (V) in metres per second, ensuring that the temporal resolution is sufficiently small to capture the relevant flow phenomena.

$$\Delta t = 0.005 - 0.01 \frac{L}{V} \tag{2}$$

2.5. Design of Experiment Using CCD–RSM

To investigate the effect of design variables (Table 3) on ship resistance in a structured manner, a Design of Experiments (DOE) framework was adopted using the Central Composite Design (CCD) technique, as shown in Table 4. CCD is a commonly applied method within the Response Surface Methodology for developing second-order polynomial models that describe the relationship between input variables and the response variable. This method reduces the amount of sample data needed to generate the mathematical model. This study used 9 samples, which is less compared to the Sobol sequence sampling in [11], which used 200 samples for 6 variables.

The independent variables consisted of geometric parameters associated with hull-form modification together with centre-of-gravity parameters governing trim adjustment. These variables were normalised and expressed in coded, dimensionless levels, where -1, 0, and +1 correspond to factorial points, while ± 1.414 represents the axial points.

To ensure numerical stability and physical accuracy in determining the vessel attitude, the initial orientation for each simulation case was defined using a two-stage equilibrium procedure. First, the hydrostatic equilibrium position for each LCG and VCG configuration was calculated to determine the theoretical trim angle. The calculated values were then used as the initial conditions in the CFD simulations.

Table 3. Design variables and codes for all scenarios.

Design Variables	−1.414	−1	0	1	1.414
	Scenario 1 (Hull Optimisation)				
LCB/LWL from FP (%), x_1	46.167	47.196	49.68	52.164	53.193
CB (-), x_2	0.532	0.543	0.572	0.601	0.612
	Scenario 2 (Trim Optimisation for Initial Hull)				
LCG (m), x_1	1.428	1.46	1.537	1.614	1.646
VCG (m), x_2	0.217	0.222	0.234	0.246	0.251
	Scenario 3 (Trim Optimisation for Optimal Hull)				
LCG (m), x_1	1.313	1.342	1.413	1.484	1.513
VCG (m), x_2	0.203	0.207	0.218	0.229	0.234

Table 4. The CCD matrix used to generate the simulation cases for the optimisation study.

Simulation Cases			Code	
Scenario 1 (Hull Optimisation)	**Scenario 2 (Trim Optimisation for Initial Hull)**	**Scenario 3 (Trim Optimisation for Optimal Hull)**	**X_1 (-)**	**X_2 (-)**
HF 0	LC 0	TR 0	0	0
HF 1	LC 1	TR 1	1	1
HF 2	LC 2	TR 2	1	−1
HF 3	LC 3	TR 3	−1	1
HF 4	LC 4	TR 4	−1	−1
HF 5	LC 5	TR 5	−1.414	0
HF 6	LC 6	TR 6	1.414	0
HF 7	LC 7	TR 7	0	−1.414
HF 8	LC 8	TR 8	0	1.414

This initial alignment was intentionally applied to keep the vessel close to its final dynamic equilibrium from the beginning of the simulation. As a result, the free-surface volume refinement region could be maintained in a relatively compact form. If the simulation had started from an even-keel condition, a much thicker refinement zone would have been required to capture the free-surface variation during the transition towards the final trim condition, which would have unnecessarily increased the total number of mesh cells.

During the simulations, the vessel was allowed to move freely in two degrees of freedom (2-DOF), namely sinkage and trim, until dynamic equilibrium was achieved. Since the vessel operates as a displacement ship at a moderate Froude number, the effect of dynamic lift was relatively small. As a result, the final dynamic trim angle differed by less than 0.005° from the initial hydrostatic condition. This approach confirms that the reported trim angles are consistent from both hydrostatic and hydrodynamic perspectives.

Within the Central Composite Design framework, each design point represents a unique combination of the selected parameters, as shown in Figures 4–6. For every combination, a CFD simulation was performed to obtain the corresponding resistance value. These simulation results were then used to develop regression models through the Re-

sponse Surface Methodology, enabling the relationship between the design variables and the resistance to be approximated mathematically.

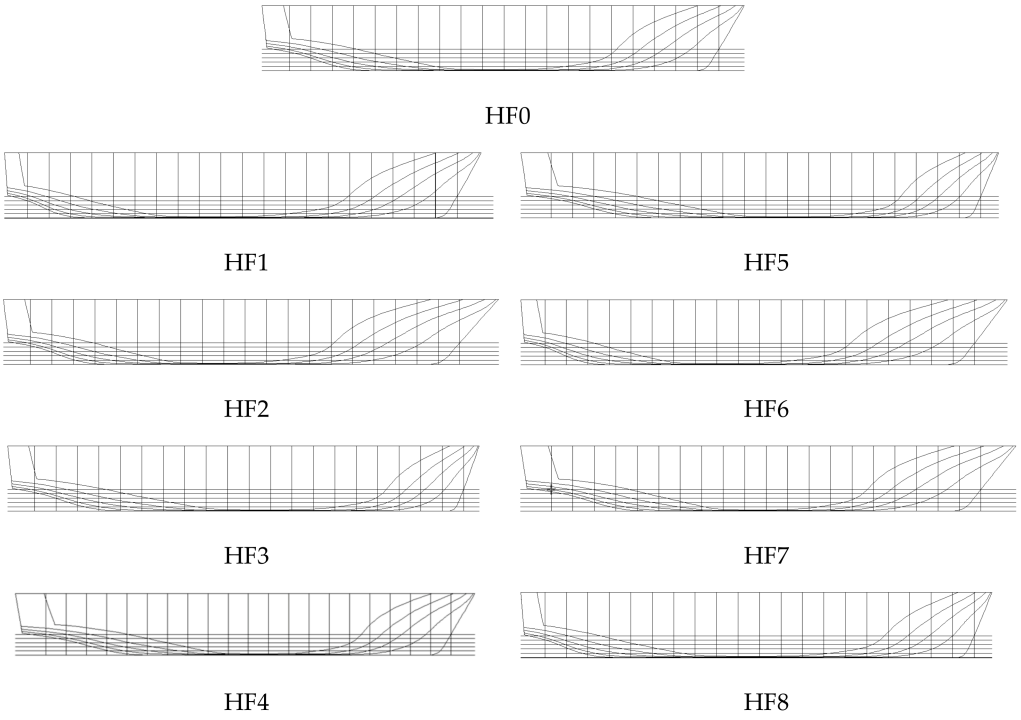


Figure 4. Hull form variation according to the CCD matrix in Table 4.

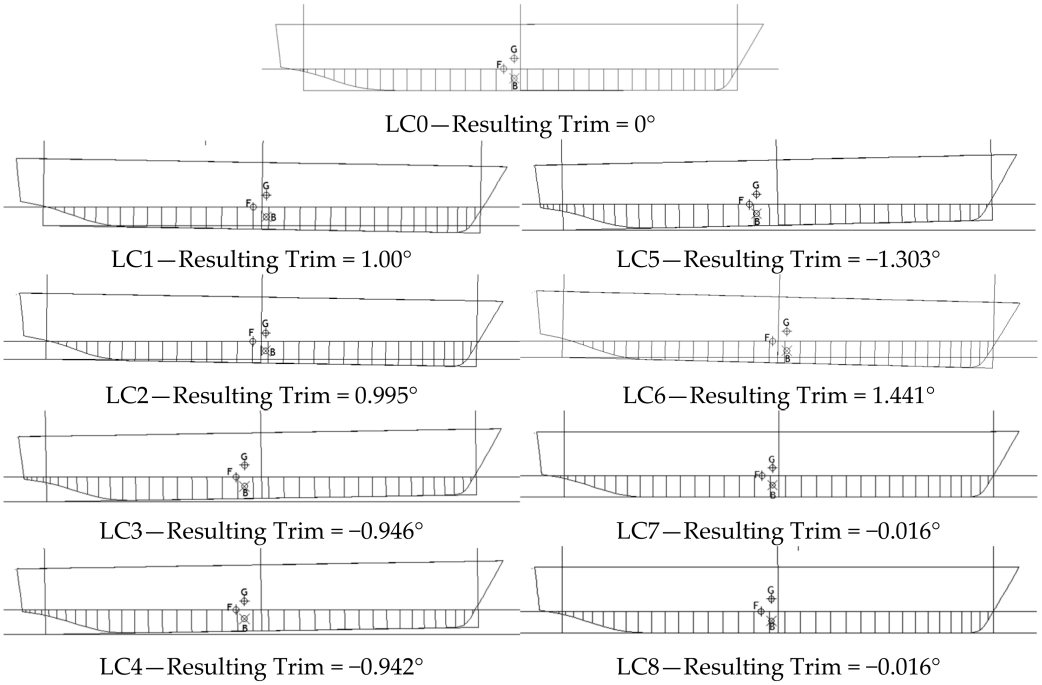


Figure 5. Trim angle variation according to the CCD matrix in Table 4.

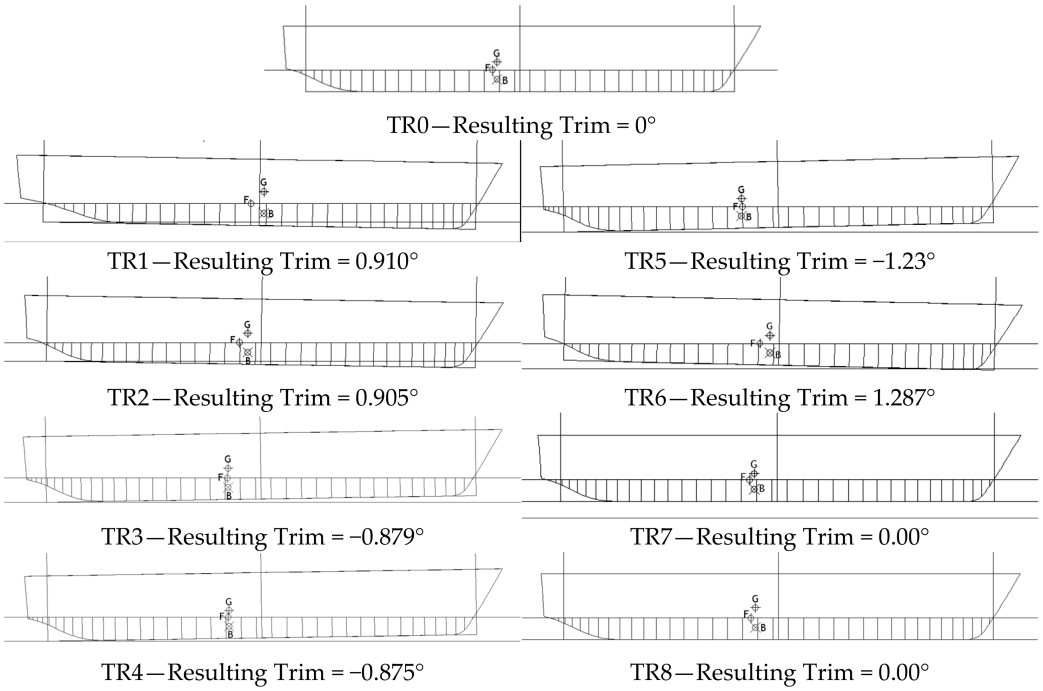


Figure 6. Trim angle of the optimal hull form variation according to the CCD matrix in Table 4.

A general representation of the second-order regression model employed in the analysis is given in Equation (3),

$$R_T(x_1, x_2) = a + bx_1 + cx_2 + d{x_1}^2 + e{x_2}^2 + fx_1x_2, \quad (3)$$

where R_T represents the total resistance, X_1 and X_2 are the independent variables, and a to f denotes the regression coefficients.

The optimal condition was obtained by evaluating the first derivative of the response function with respect to each variable, as presented in Equation (4). This procedure results in a system of two linear equations with two unknowns, the solution of which identifies the stationary point (x_1, x_2). To ensure that the resulting optimum remains within a physically meaningful range, constraints were imposed on the variables. In this study, both variables were limited to a range of ± 2.5 in coded units, which corresponds to a deviation of $\pm 12.5\%$ from the initial design values.

$$R_{T\ min}(x_1, x_2) = \frac{dR_T(x_1, x_2)}{dx_1} = 0\ R_{T\ min}(x_1, x_2) = \frac{dR_T(x_1, x_2)}{dx_2} = 0 \quad (4)$$

3. Results and Discussion

3.1. Accuracy and Numerical Uncertainty of the CFD Model

3.1.1. Model Validation (Accuracy)

The accuracy of the numerical model was rigorously validated by comparing the CFD resistance predictions with available experimental data across a speed range equivalent to 12 to 17 knots at full scale. The comparison reveals an excellent correlation between the two datasets, with the numerical model consistently following the physical trends observed in the experiments. As the vessel speed increases, the CFD model demonstrates high fidelity in capturing the hydrodynamic resistance, ensuring that the chosen physics models and boundary conditions are representative of the actual fluid flow, as shown in Table 5 and Figure 7.

Table 5. Comparison of total resistance between CFD results and experimental test results.

V Ship (knot)	V Model (m/s)	Fr	Experimental Data (N)	CFD Results (N)	Difference (%)
12	1.455	0.26	11.37	10.991	−3.33
13	1.576	0.28	14.29	14.112	−1.25
14	1.698	0.30	18.54	18.358	−0.98
15	1.819	0.32	22.96	22.617	−1.49
16	1.94	0.34	28.06	27.716	−1.23
17	2.061	0.36	35.91	35.554	−0.99
Mean Absolute Percentage Error (MAPE)					1.545%
Root Mean Square Error (RMSE)					0.309 N
Mean Absolute Error (MAE)					0.297 N

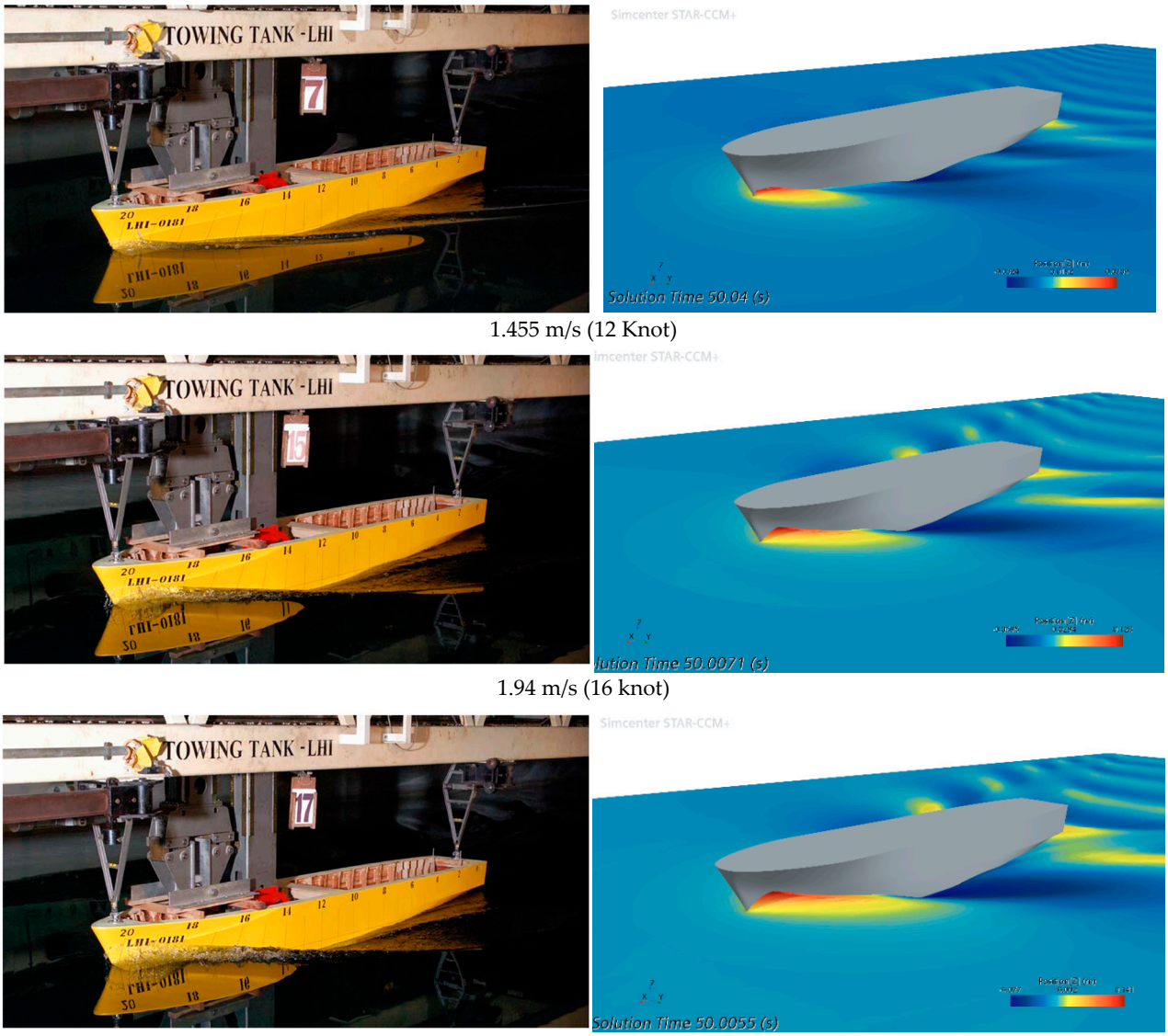


Figure 7. Visual comparison between CFD results and experimental test results.

3.1.2. Numerical Uncertainty (Grid and Time-Step Convergence)

To ensure the reliability of the numerical results, a systematic convergence study was conducted. The fine configuration was first validated by comparing its numerical results with the experimental data. To perform the Grid Convergence Index (GCI) analysis shown in Table 6, this validated fine configuration was then systematically coarsen into medium and coarse configurations by adjusting both the spatial grid size and temporal discretisation. This approach is based on the Richardson extrapolation [29] as described by [30]. This dual-refinement approach was essential to maintaining a consistent Courant–Friedrichs–Lewy (CFL) number across all test cases, thereby ensuring that numerical stability and the Courant number remained uniform as the mesh density increased [31]. Three configurations, fine, medium, and coarse, were evaluated, with total cell counts of 1,646,201, 762,315, and 402,572, respectively. The time steps were adjusted proportionally from 0.0450 s for the coarse mesh to 0.0225 s for the fine mesh to satisfy the requisite temporal resolution criteria.

Table 6. Mesh configurations used in the grid convergence study.

Fine configuration	Total cells = 1,646,201, time step = 0.0225 s
Medium configuration	Total cells = 762,315, time step = 0.03182 s
Coarse configuration	Total cells = 402,572, time step = 0.0450 s
Fine solution, S_1	10.9906 N
Medium solution, S_2	11.0844 N
Coarse solution, S_3	11.4671 N
Medium–fine, ε_{21}	0.0939
Coarse–medium, ε_{32}	0.3827
Convergence ratio, R	0.2453
Order of accuracy, p	4.0546
GCI (%)	0.3472

The verification process revealed stable numerical behaviour as the space–time resolution was increased. The calculated convergence ratio (R) was 0.2453, which falls within the range of $0 < R < 1$, indicating that the solution achieves monotonic convergence. Furthermore, the calculated order of accuracy (p) was found to be 4.0546. These metrics confirm that the differences between the solutions S_1, S_2, and S_3 diminish consistently, suggesting that the numerical model is robust and the flow physics are effectively captured by the discretisation scheme.

The Grid Convergence Index (GCI) was applied to quantify the numerical uncertainty of the fine-grid solution. The GCI for the fine configuration was determined to be 0.3472%, a remarkably low value which indicates that the results are effectively independent of further grid or time-step refinement. This negligible uncertainty level provides high confidence in the numerical framework. Consequently, the fine configuration was adopted for all subsequent simulations, as it offers a superior balance between high-fidelity precision and computational economy.

3.2. Statistical Analysis of CCD–RSM

Following the numerical verification and validation of the CFD model, a comprehensive statistical analysis was performed to evaluate the relationship between the design variables and the ship's performance characteristics. This section details the application of the Central Composite Design (CCD) and Response Surface Methodology (RSM) to de-

velop a high-fidelity meta-model of hull performance. The subsequent subsections present a rigorous assessment of the model's quality, beginning with the regression statistics to determine the goodness of fit, followed by an Analysis of Variance (ANOVA) to verify the internal consistency of the data. Finally, the individual model coefficients are examined to identify the significance of each design parameter and their potential interactions, ensuring that the mathematical model is robust enough for subsequent multi-objective optimisation.

3.2.1. Regression Statistic

The predictive capability of the developed RSM models was initially evaluated through a detailed assessment of the regression statistics for the three proposed scenarios. As summarised in Table 7, all scenarios exhibit exceptionally high coefficients of determination, with R^2 values exceeding 0.994. This indicates that the models can account for more than 99.4% of the variance in the response data, demonstrating a near-perfect fit between the numerical observations and the regression surfaces. Furthermore, the Adjusted R^2 values for all cases remain above 0.985, confirming that the high degree of accuracy is not merely a result of over-fitting but a reflection of the models' inherent robustness across the nine observations conducted for each scenario.

Table 7. Regression statistics for the three scenarios.

Variables	Scenario 1 (Hull Optimisation)	Scenario 2 (Trim Optimisation for Initial Hull)	Scenario 3 (Trim Optimisation for Optimal Hull)
Multiple R	0.997987179	0.997197493	0.999076442
R Square	0.995978409	0.994402841	0.998153737
Adjusted R Square	0.989275758	0.985074242	0.995076631
Standard Error	0.071647131	0.048578822	0.026297284
Observations	9	9	9

A comparative analysis of the three scenarios reveals subtle but significant differences in their statistical precision. Scenario 1 (Hull Optimisation) and Scenario 2 (Trim Optimisation for Initial Hull) show strong performance, with Multiple R values of 0.9979 and 0.9971, respectively. However, it is noteworthy that Scenario 2 yields a lower standard error (0.0486) compared to Scenario 1 (0.0716), suggesting that the response surface for trim optimisation on the initial hull form is slightly more stable. Nevertheless, both scenarios provide a highly reliable basis for predicting hydrodynamic performance within their respective design spaces.

Among the three scenarios, Scenario 3 (Trim Optimisation for an Optimal Hull) emerges as the best model in terms of statistical fidelity. It achieves the highest Multiple R (0.9991) and R^2 (0.9982), coupled with an Adjusted R^2 of 0.9951. Crucially, Scenario 3 exhibits the lowest standard error at only 0.0263, which is significantly lower than that of the other two scenarios. This enhanced precision indicates that the interaction between the optimal hull geometry and the active trim parameters is captured with remarkable accuracy by the meta-model. Consequently, Scenario 3 offers the most reliable predictive framework for the final stages of the optimisation process.

3.2.2. Analysis of Variance

An Analysis of Variance (ANOVA) was performed to rigorously evaluate the statistical significance of the regression models developed for the three scenarios. As presented in Table 8, the ANOVA results confirm that all three models are statistically significant, pro-

viding a high degree of confidence in the relationship between the design variables and the predicted performance metrics. The degrees of freedom (df) were consistently maintained across all scenarios, with five degrees of freedom for the regression and three for the residuals, resulting in a total of eight degrees of freedom for the nine observations conducted.

Table 8. Analysis of Variance (ANOVA).

Component	df	SS	MS	F	Significance F
Scenario 1 (Hull Optimisation)					
Regression	5	3.813914072	0.762782814	148.5946904	0.000862784
Residual	3	0.015399934	0.005133311		
Total	8	3.829314006			
Scenario 2 (Trim Optimisation for Initial Hull)					
Regression	5	1.257795136	0.251559027	106.5972373	0.001414618
Residual	3	0.007079706	0.002359902		
Total	8	1.264874842			
Scenario 3 (Trim Optimisation for Optimal Hull)					
Regression	5	1.121622843	0.224324569	324.3807285	0.000268904
Residual	3	0.002074641	0.000691547		
Total	8	1.123697484			

A critical indicator of the model's performance is the Significance F value, which in all three cases is substantially lower than the standard threshold of 0.05. Specifically, Scenario 3 exhibits the most favourable result, with a Significance F value of 0.00027, followed by Scenario 1 (0.00086) and Scenario 2 (0.00141). These exceptionally low values indicate that the probability of the regression results occurring by chance is extremely remote, thereby validating the statistical adequacy of the Response Surface Methodology (RSM) models for predicting ship performance.

Furthermore, the high F-statistic values observed across the scenarios, peaking at 324.38 for Scenario 3, further reinforce the robustness of the models. The significantly higher mean square (MS) for the regression components compared to the residuals suggests that the model effectively captures the underlying trends of the data rather than being influenced by stochastic noise. Consequently, the ANOVA results provide strong empirical evidence that the developed RSM meta-models are reliable tools for capturing the hydrodynamic characteristics of the hull, with the third scenario demonstrating the most pronounced statistical precision.

3.2.3. Regression Coefficients and Statistical Significance

In Table 9, the significance of the individual regression coefficients is evaluated using *p*-values to determine the impact of each design variable on the ship's hydrodynamic performance. In Scenario 1 (Hull Optimisation), all variables, including linear terms (X_1, X_2), quadratic terms ($X_1{}^2$, $X_2{}^2$), and the interaction term (X_1X_2), demonstrate a high degree of statistical significance, with *p*-values notably lower than 0.05. This suggests that the hull geometry optimisation is highly sensitive to both primary variables (LCB and Cb) and their complex interactions, necessitating the inclusion of a full second-order polynomial model to capture the non-linear behaviour of the resistance response surface accurately.

Table 9. Coefficient model and its significance.

Variable	Scenario 1 (Hull Optimisation)		Scenario 2 (Trim Optimisation for Initial Hull)		Scenario 3 (Trim Optimisation for Optimal Hull)	
	Coefficients	***p*-Value**	**Coefficients**	***p*-Value**	**Coefficients**	***p*-Value**
Intercept	10.9906	0.0000	10.9906	0.0000	10.735	0.0000
X_1	−0.6110	0.0002	0.3939	0.0002	0.3740	0.0000
X_2	0.1985	0.0043	0.0090	0.6364	0.0102	0.3548
${X_1}^2$	0.2756	0.0072	0.0592	0.1292	0.0069	0.6866
${X_2}^2$	0.1144	0.0724	0.0040	0.8977	0.0003	0.9870
X_1X_2	−0.2616	0.0053	0.0078	0.7692	−0.0207	0.2129

In contrast, Scenarios 2 and 3, which focus on trim optimisation, exhibit a markedly different sensitivity profile. In these instances, only the linear term X_1 (LCG) maintains statistical significance ($p < 0.0001$), while the quadratic and interaction terms return p-values significantly higher than the 0.05 threshold. This indicates that for the trim optimisation phase, whether applied to the initial or the optimal hull, the relationship between the design variables and resistance is predominantly linear. Consequently, the higher-order terms do not contribute meaningfully to the model's predictive accuracy in these scenarios, suggesting that a simpler, reduced-order model would suffice for trim adjustments.

$$RT\ (N) = 10.9906 - 0.611x_1 + 0.1985x_2 + 0.2756{x_1}^2 + 0.1144{x_2}^2 - 0.2616x_1x_2 \quad (5)$$

$$RT\ (N) = 10.9906 + 0.3939x_1 + 0.009x_2 + 0.0592{x_1}^2 + 0.004{x_2}^2 - 0.0078x_1x_2 \quad (6)$$

$$RT\ (N) = 10.735 + 0.374x_1 + 0.0102x_2 + 0.0069{x_1}^2 + 0.0003{x_2}^2 - 0.0207x_1x_2 \quad (7)$$

The coefficients for every scenario provide mathematical models (Equations (5)–(7), respectively) and critical insights into the design space characteristics. It should be noted that Equations (5)–(7) can be used when X_1 and X_2 (design variables) are in code form. The negative coefficient for X_1 (LCB) in Scenario 1 suggests an inverse relationship between the primary variable and resistance during the hull form development. As the measurement of LCB in this case is calculated from FP as the percentage from LWL, negative results mean shifting LCB forward. Meanwhile, the positive coefficients in Scenarios 2 and 3 reflect the trend during trim optimisation. The substantial reduction in p-values for the higher-order terms in the trim scenarios confirms that the optimisation landscape becomes more regular and less non-linear once the optimal hull form is established. This statistical distinction validates the tiered approach to the optimisation process, ensuring that the model's complexity is appropriately matched to the physical requirements of each scenario.

3.3. Scenario 1: Hull Form Optimisation Results

The following section presents the findings from the hull form optimisation process, focusing on the identification of the optimal geometry that minimises total resistance. By leveraging the response surface generated in the previous section, the design space was explored to determine the optimal configuration of the longitudinal centre of buoyancy (LCB), represented as the percentage of LCB/LWL from FP, and the block coefficient (Cb). The results are evaluated in two parts: first, by detailing the optimal solution and its corresponding performance improvements, and second, by analysing the underlying hydrodynamic characteristics from the CFD results, such as wave patterns and pressure distribution, that contribute to the resistance reduction achieved by the optimised hull form.

3.3.1. Optimal Solution and Response Surface Analysis for Scenario 1

The optimisation process successfully identified a superior hull form configuration, referred to as 'HF 9', which demonstrates a clear improvement over the initial design. As shown in Figure 8, the response surface analysis allows for the visualisation of the resistance landscape across the defined design space of LCB (X_1) and Cb (X_2). The initial design, positioned at the origin of the design variables, resides within a region of moderate resistance; however, the optimisation algorithm directed the design towards the 'Optimal' code (1.524, 0.875), which corresponds to a percentage of LCB/LWL from FP of 53.464% and a Cb of 0.597. The comparison between initial and optimal hull form is shown in Figure 9.

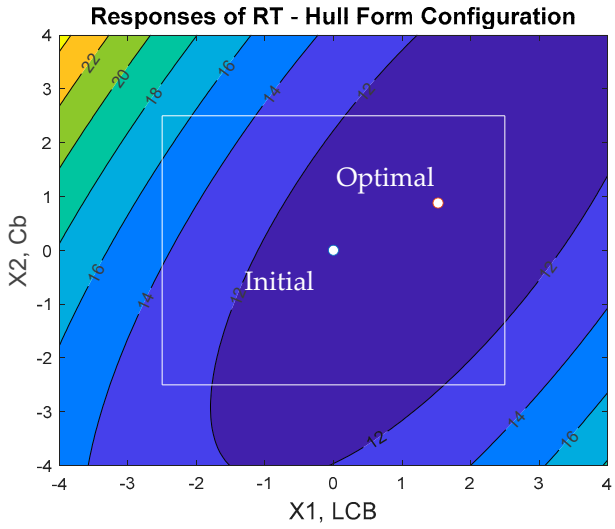
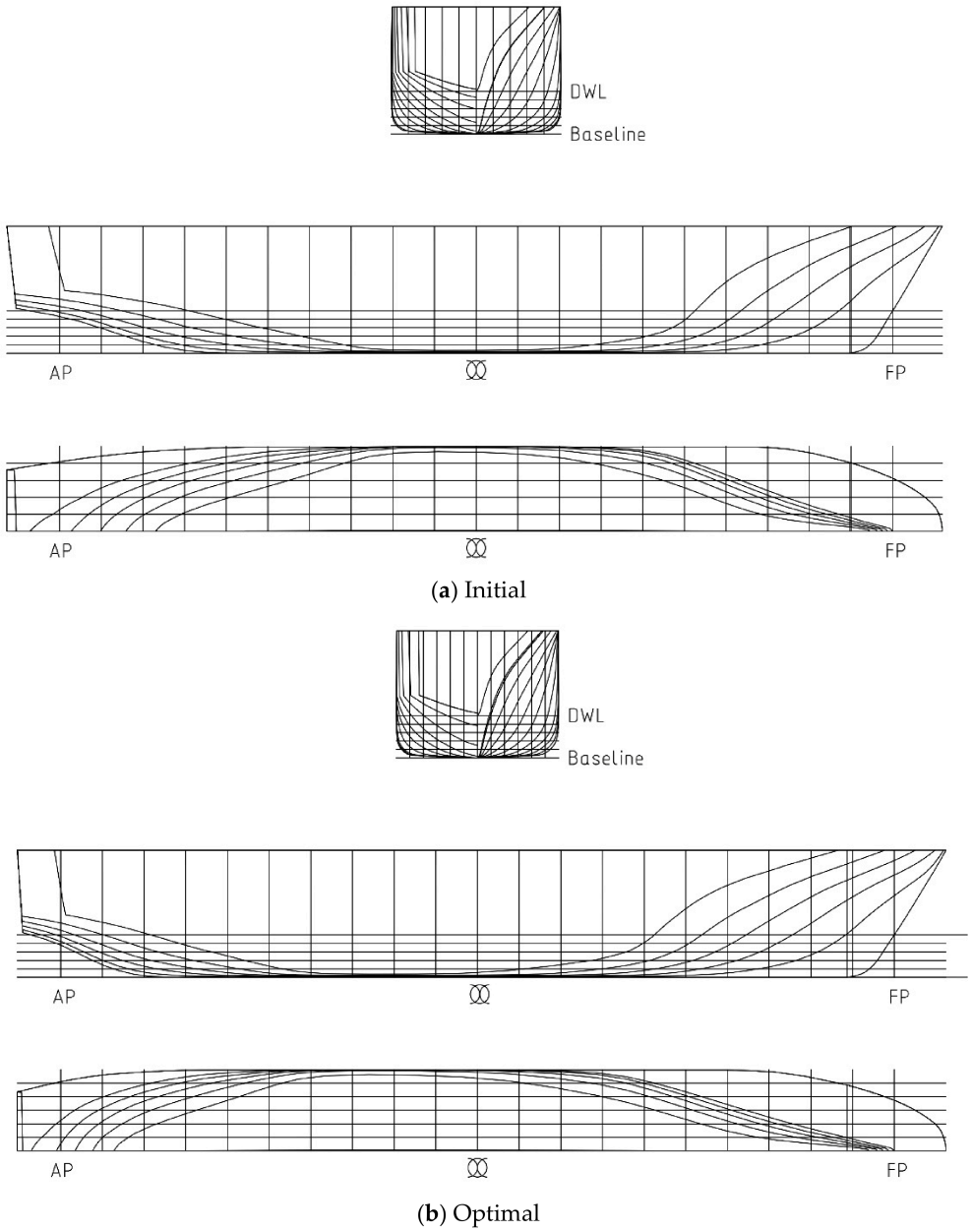


Figure 8. Response surface for Scenario 1 (Hull Form Optimisation).

Quantitatively, the transition from the initial hull to the optimal configuration yielded a notable reduction in total resistance, as shown in Table 10. The CFD results indicate that the resistance decreased from 10.991 N to 10.735 N, representing a direct performance improvement of 2.329%. This result is consistent with the regression-based prediction (Equation (5)), which estimated a more conservative reduction of 3.448%. The alignment between the CFD results and the mathematical model underscores the efficacy of the Response Surface Methodology (RSM) in navigating the design space to locate the global minimum for total resistance.

Table 10. Resistance comparison for Scenario 1 (Hull Form Optimisation).

Cases	Code		% LCB/LWL from FP	Cb (-)	RT CFD (N)	RT Equation (5) (N)
HF 0	0	0	49.68	0.572	10.991	10.991
HF 9 (Optimal HF)	1.524	0.875	53.464	0.597	10.735	10.612
				Difference (%)	−2.329	−3.448



(**a**) Initial

(**b**) Optimal

Figure 9. Side view of the initial hull and optimal hull.

Furthermore, the response surface map reveals that the resistance change is highly sensitive to changes in the LCB position, whereas the influence of Cb appears more stable within the examined range. The clear separation between the initial and optimal points on the contour plot confirms that the optimisation process effectively moved the hull form into a lower-energy configuration. This optimal point represents a balanced compromise between the volumetric requirements of the hull and the hydrodynamic necessity of minimising wave-making resistance, thereby validating the design modifications as a successful outcome of the Hull Form Optimisation strategy.

3.3.2. Hydrodynamic Characteristics of the Optimised Hull

The decomposition of the total resistance into its primary components, pressure and shear resistance, provides a clearer understanding of the hydrodynamic benefits gained from the hull form optimisation. As illustrated in Figure 10, the initial hull form exhibits a total resistance dominated by viscous effects, with pressure resistance of 3.2273 N. Following the optimisation of the longitudinal centre of buoyancy (LCB) and the block

coefficient (Cb), the pressure resistance for the optimal hull form decreased to 3.0189 N. This reduction indicates that the refined geometry effectively streamlines the flow, reducing the energy lost to wave-making and form drag, which are the primary contributors to the pressure component in pioneer vessels of this displacement.

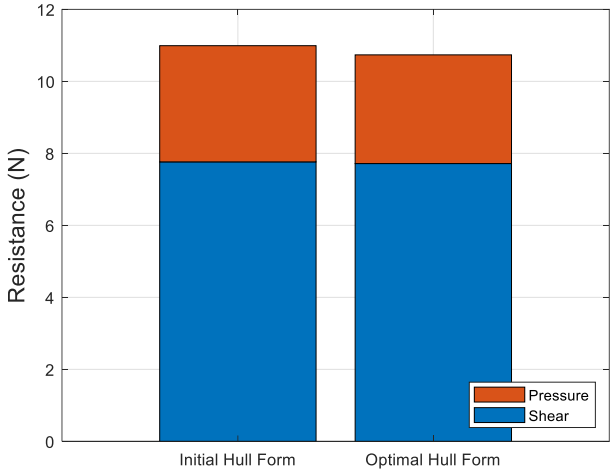


Figure 10. Comparison of resistance for the initial and optimal hull form. Initial hull form—pressure = 3.2273 N, shear = 7.7633 N; optimal hull form—pressure = 3.1132 N, shear = 7.7488 N.

In contrast, the shear resistance, representing the viscous friction between the water and the hull surface, shows a much more modest decline, decreasing from 7.7633 N to 7.7165 N. This marginal change suggests that while the wetted surface area was slightly influenced by the geometric modifications, the primary driver for the overall 2.329% efficiency gain in Scenario 1 is the improvement in the hull's pressure distribution. The result confirms that the optimisation strategy successfully targeted the vessel's form-related losses without adversely affecting the frictional profile. This redistribution of resistance components validates the use of LCB and Cb as the primary design variables for enhancing the hydrodynamic efficiency of this pioneer ship.

The comparative analysis of the pressure distribution on the hull surface provides clear physical evidence of the improvements in the vessel's form drag, as depicted in the top half of Figure 11. The CFD simulations reveal that the initial hull form experiences a higher stagnation pressure concentration, indicated by the deeper orange-red region at the bow, inside the white box. In contrast, the optimal hull form, with its refined LCB and block coefficient (Cb), shows a distinct reduction in this peak pressure area. This indicates that the geometric modifications successfully streamlined the flow around the bow, effectively lessening the total resistance experienced by the pioneer ship.

This pressure reduction is not limited to the bow but also shows improved distribution along the vessel's length and at the transom. The broader blue and green bands along the midsection of the optimal hull (inside the white box) suggest a more stable pressure recovery compared to the initial design. This leads to a decreased pressure differential between the forward and aft sections, which is the primary driver of form drag. This visual data directly correlates with the statistical finding that the geometric refinements in Scenario 1 targeted and successfully mitigated form-related losses, thereby confirming the statistical adequacy of the regression model.

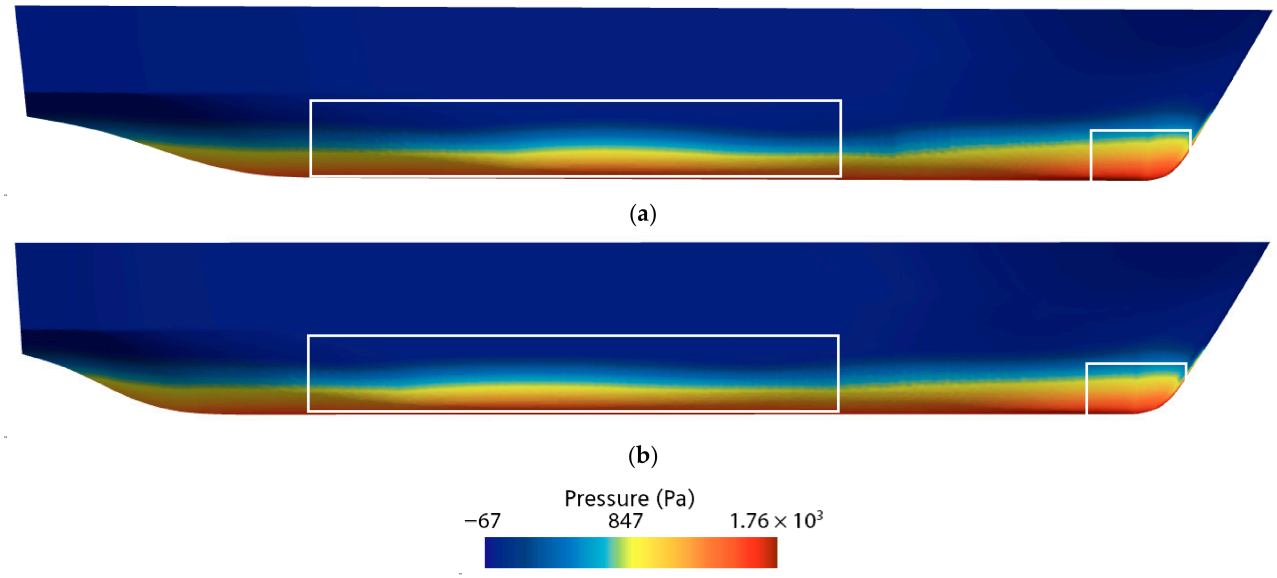


Figure 11. Pressure distribution of the initial hull form, HF 0 (**a**), and optimal hull form, HF 9 (**b**). The white boxes indicate the specific regions of interest for pressure distribution comparison.

Turning to the visual analysis of the wave patterns, the Volume Fraction of Air (VFA) contours in the bottom half of Figure 12 illustrate the free surface deformation, providing a clear visualisation of the wave elevation. The VFA contour clearly marks the air–water interface, where the initial hull design generates a more pronounced, steep wave profile at the bow (the orange-to-white region). This steeper wave signifies a greater energy transfer from the ship's forward motion to the formation of the wave system, directly contributing to high wave-making resistance, a critical component for displacement vessels of this type.

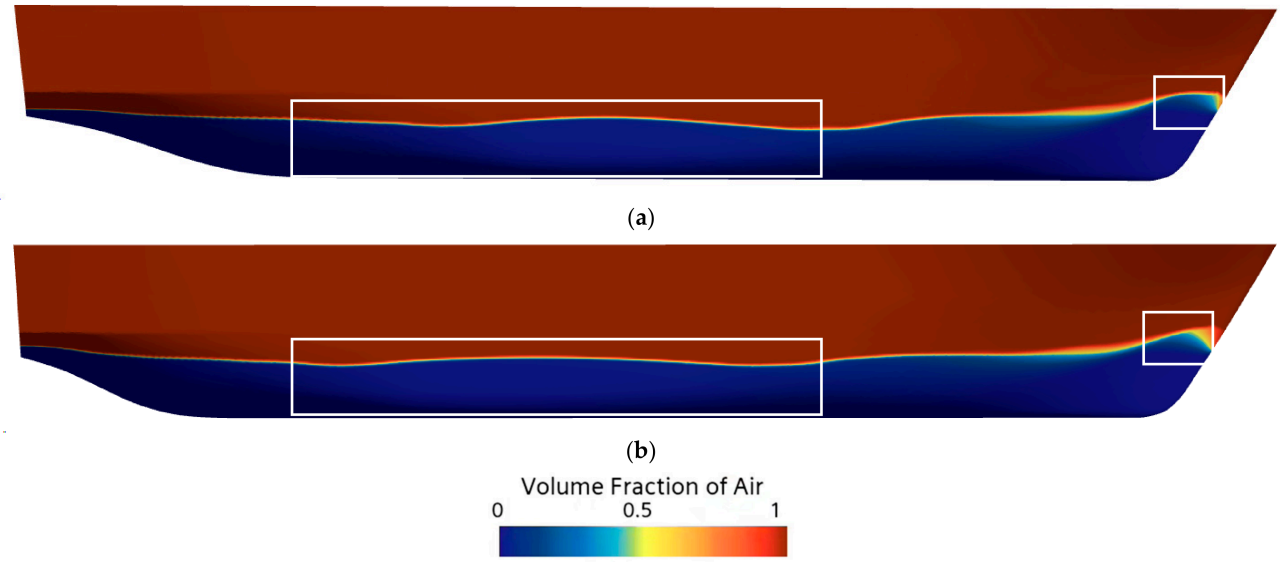


Figure 12. Free surface contour at the hull with the initial hull form, HF 0 (**a**), and optimal hull form, HF 9 (**b**). The white boxes indicate the specific regions of interest for free surface comparison.

Conversely, the optimal hull design produces a visibly flatter and more refined wave profile. This indicates that the modifications in LCB and Cb produce a better hydrodynamic match for the vessel's speed, reducing the energy lost to the creation of larger, more aggressive waves. By decreasing the amplitude and steepness of the bow wave, the optimal hull form achieves superior efficiency, validating the reduction in total resistance

observed in the numerical results. This synergistic relationship between reduced pressure concentrations and a smoother wave profile underscores the physical mechanism that leads to the successful optimisation of the hull geometry in Scenario 1.

3.4. Scenario 2: Trim Optimisation Results (Initial Hull)

Following the hull form modification, this study investigated the impact of trim on the initial vessel's total resistance. This section examines Scenario 2, where the vessel's longitudinal centre of gravity (LCG) and vertical centre of gravity (VCG) were adjusted to find the optimal static trim configuration. By decoupling the trim effects from the hull form changes, this analysis provides a clear baseline for understanding how much resistance can be mitigated through loading and balance adjustments alone, prior to any geometric alterations.

3.4.1. Optimal Solution and Response Surface Analysis for Scenario 2

The trim optimisation for the initial hull form focused on determining the ideal balance between LCG (X_1) and VCG (X_2) to minimise total resistance (RT). As illustrated in the response surface in Figure 13, the resistance landscape exhibits a strong sensitivity to the LCG position, with the contour lines indicating a significant reduction in resistance as the LCG is shifted forward. The initial condition, located at the centre of the design space, was compared with the 'Optimal' configuration, which the algorithm identified at the code (−2.5, 1.318). This shift corresponds to an LCG adjustment to 1.345 m and a VCG of 0.249 m.

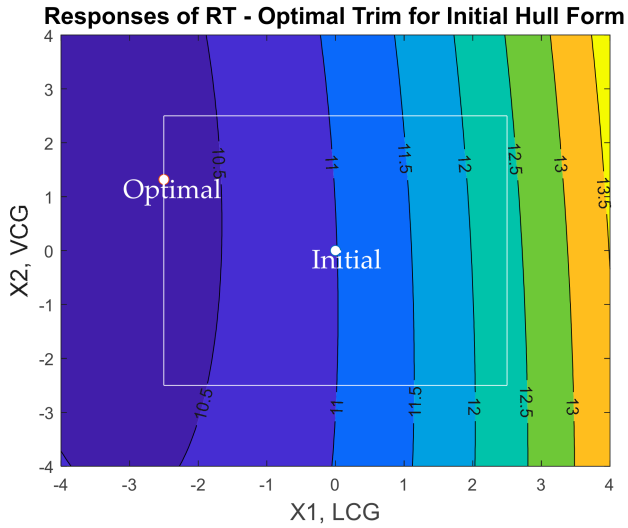


Figure 13. Response surface for Scenario 2 (Trim Optimisation for Initial Hull Form).

The implementation of this optimal trim configuration resulted in a reduction in total resistance from 10.991 N to 10.861 N, based on the CFD simulations. This equates to a performance gain of 1.183% (Table 11). Although this improvement is more modest than that achieved through hull form modification in Scenario 1, it confirms that trim optimisation can provide a meaningful reduction in resistance without requiring structural changes. The regression model (Equation (6)) predicted a more substantial reduction of 5.659%; while the CFD result is more conservative, both methods agree on the direction and location of the optimal point within the design space.

Table 11. Resistance comparison for trim optimisation for the initial hull form.

Cases	Code		LCG (m)	VCG (m)	RT CFD (N)	RT Equation (6) (N)
LC 0	0	0	1.537	0.234	10.991	10.991
LC 9 (Optimal Trim)	−2.5	1.318	1.345	0.249	10.861	10.369
				Difference (%)	−1.183	−5.659

A closer inspection of Figure 13 reveals that the VCG (X_2) has a relatively negligible impact on resistance compared to the LCG, as evidenced by the near-vertical orientation of the contour lines. This suggests that the hydrodynamic performance of the initial hull is primarily governed by the longitudinal distribution of weight, which directly influences the running trim and wetted surface area. By shifting the LCG to the 'Optimal' position (LC 9), the vessel achieves a more efficient hydrodynamic trim, effectively reducing the pressure drag and yielding a more favourable resistance profile for the initial hull configuration.

3.4.2. Hydrodynamic Characteristics of the Initial Hull with Optimal Trim

The impact of active trim control on the resistance components of the initial hull form is illustrated in Figure 14. By adjusting the longitudinal and vertical centres of gravity (LCG and VCG) to achieve the optimal running trim, a reduction in total resistance was observed, primarily driven by the pressure component. The CFD analysis indicates that the pressure resistance decreased from 3.2273 N in the initial trim condition to 3.1132 N in the optimal trim configuration. This reduction suggests that even without geometric modifications to the hull, the vessel's pressure field can be effectively managed by optimising its static trim, leading to a more efficient interaction between the hull and the free surface.

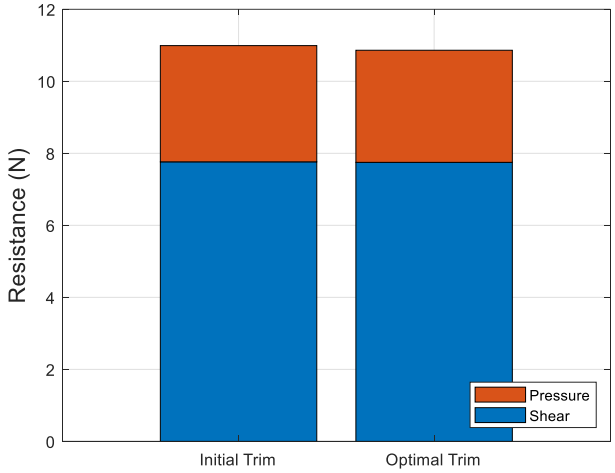
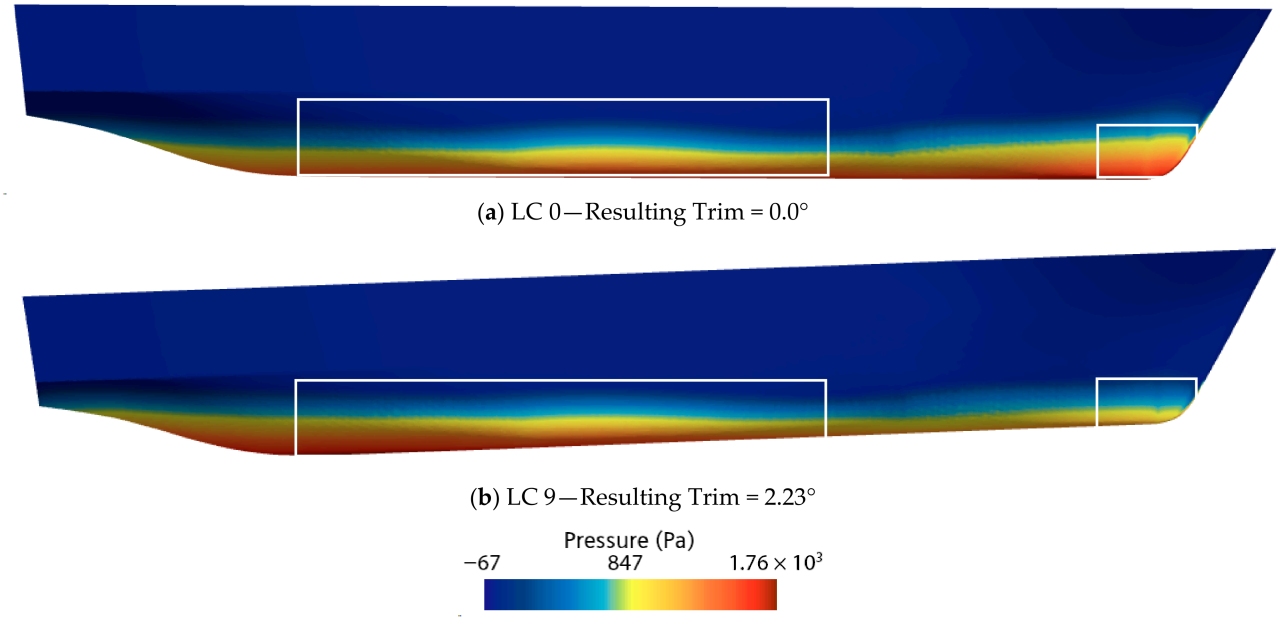


Figure 14. Comparison of resistance for the initial trim and optimal trim. Initial trim—pressure = 3.2273 N, shear = 7.7633 N; optimal trim—pressure = 3.1132 N, shear = 7.7488 N.

Consistent with the trends observed in the previous scenario, the shear resistance remained relatively stable, experiencing only a minor decrease from 7.7633 N to 7.7488 N. This marginal change confirms that the optimisation of the trim primarily influences the form-related losses rather than significantly altering the wetted surface area or the viscous friction profile of the vessel. These results validate Scenario 2 as a highly effective operational strategy; by fine-tuning the vessel's trim, the pressure drag can be lowered,

providing a meaningful enhancement in hydrodynamic efficiency for the existing hull form without the need for structural alterations.

The visual analysis of the pressure distribution, as presented in Figure 15, elucidates the physical mechanism behind the reduction in pressure resistance from 3.2273 N to 3.1132 N. In the 'Initial' condition, the hull exhibits a broader and more intense stagnation zone at the bow, where the high-pressure field (red contour) extends significantly upward. Upon implementing the optimal trim, there is a visible downward and aft redistribution of this pressure field. This transition indicates that the vessel has adopted a more streamlined dynamic trim, which effectively lowers the stagnation pressure peak at the forward section and leads to a more favourable pressure recovery along the hull's midbody.



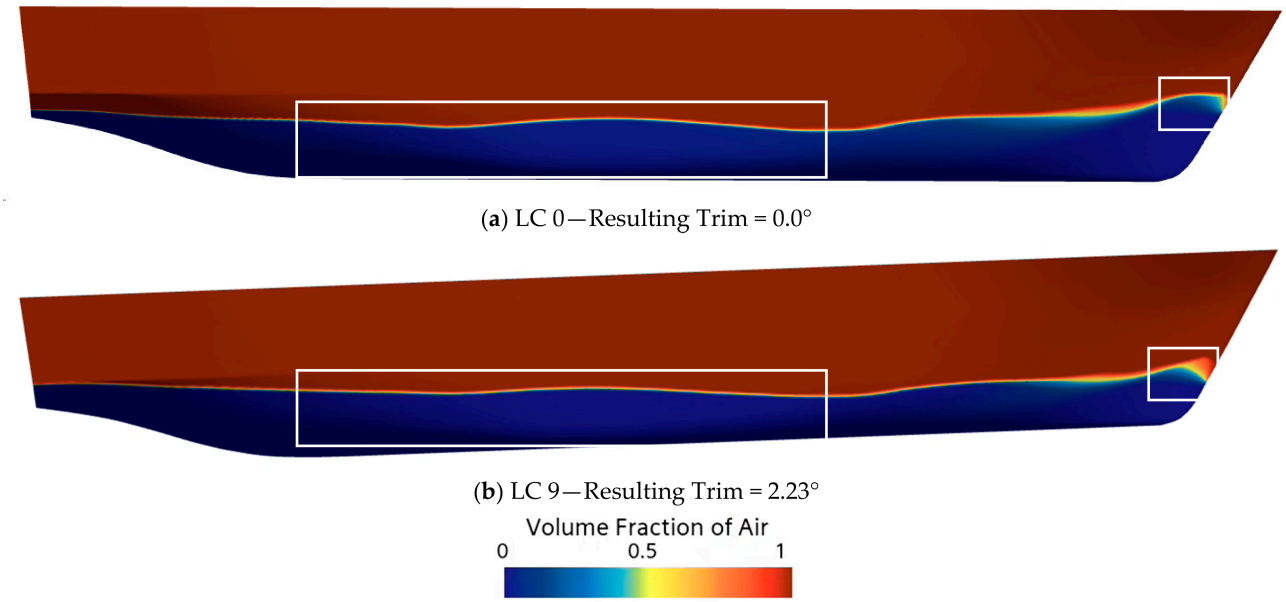
(**a**) LC 0—Resulting Trim = 0.0°

(**b**) LC 9—Resulting Trim = 2.23°

Figure 15. Pressure distribution of the initial trim, LC 0 (**a**), and optimal trim, LC 9 (**b**). The white boxes indicate the specific regions of interest for pressure distribution comparison.

Quantitatively, the visual data in Figure 15 confirms that the optimal running trim for the initial hull involves a bow-up trim of 2.23°. This shift in the deck's inclination is evidenced by the altered alignment of the pressure contours relative to the design waterline. By lifting the bow by 2.23 degrees, the vessel reduces the hydrostatic immersion of its blunter forward sections. This change in trim is the primary driver for the 1.183% reduction in total resistance, as it allows the hull to slice through the water at a more efficient angle of attack, thereby mitigating the form drag that previously hindered the vessel's progress at the design speed.

The impact of this 2.23° trim adjustment is further validated by the wave pattern analysis shown in the Volume Fraction of Air (VFA) contours in Figure 16. In the initial trim state, the interaction between the bow and the free surface creates a steep, high-amplitude wave crest, indicating significant energy dissipation into the wave system. However, in the optimal state, the 2.23-degree bow-up inclination results in a visibly flatter and more elongated wave profile. This smoothing of the air–water interface suggests a reduction in wave-making resistance, which is a key component of the overall pressure drag for pioneer ships in this speed range.



(**a**) LC 0—Resulting Trim = 0.0°

(**b**) LC 9—Resulting Trim = 2.23°

Figure 16. Free surface contour at the hull with the initial trim, LC 0 (**a**), and optimal trim, LC 9 (**b**). The white boxes indicate the specific regions of interest for free surface comparison.

Furthermore, the consistency in the shear resistance (minimally changed from 7.7633 N to 7.7488 N) is reflected in the VFA contours, which show that the total wetted surface remains largely unchanged despite the 2-degree tilt. This confirms that the hydrodynamic benefits of Scenario 2 are almost entirely derived from the optimisation of the pressure field and wave system rather than a frictional reduction. The synergy between the 2.23-degree trim and the resulting flatter wave profile, as shown in Figure 16, provides a robust physical justification for the predictive accuracy of the RSM model and highlights the efficacy of trim management as a critical operational strategy for enhancing vessel efficiency.

3.5. Scenario 3: Integrated Optimisation Results (Trim Optimisation for Optimised Hull Form)

The final stage of this study involves Scenario 3, which investigates the trim optimisation for the optimised hull form (HF 9). By applying trim optimisation to a vessel geometry that has already been refined, this section aims to identify the global minimum for total resistance within the combined design space. This multi-stage approach determines whether further hydrodynamic gains can be extracted from an already efficient hull form through precise adjustments of the longitudinal and vertical centres of gravity.

3.5.1. Optimal Solution and Response Surface Analysis for Scenario 3

The integrated optimisation of the refined hull form focuses on the interaction between the optimal geometry and the loading parameters, specifically LCG (X_1) and VCG (X_2). As demonstrated in the response surface in Figure 17, the resistance contours show a significant downward trend as the LCG is shifted further aft and the VCG is lowered. The optimal code for this scenario was identified at the extreme boundary of the design space with coordinates of (−2.5, −2.5), corresponding to an LCG of 1.236 m and a VCG of 0.191 m. This suggests that for the optimised hull, a more aggressive trim adjustment is required to achieve peak efficiency compared to the initial design.

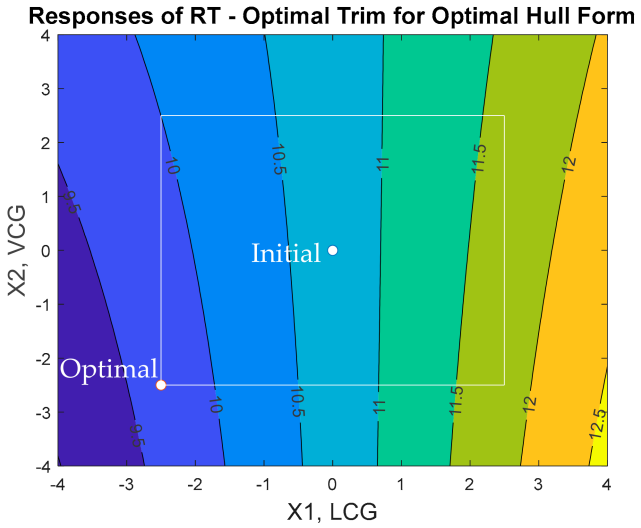


Figure 17. Response surface for Scenario 3 (Trim Optimisation for Optimal Hull Form).

Although this may indicate that a lower mathematical optimum could exist outside the current range, the LCG and VCG limits were deliberately set based on practical naval architecture and operational constraints for pioneer ships. Extending these variables further could create impractical loading conditions, such as excessive trim, reduced propeller submergence, poor bridge visibility, and arrangement issues. Therefore, the result is considered a practical constrained optimum. The RSM model remains valid within these realistic boundaries and provides a feasible design solution that balances hydrodynamic performance with operational requirements.

The quantitative results for Scenario 3 represent the most substantial reduction in resistance achieved in this study. The total resistance was reduced from 10.735 N (for the optimal hull with the initial trim) to 10.135 N (for the optimal hull with the optimal trim), as shown in Table 12. This indicates a 5.589% improvement from the already optimised state. More significantly, when compared to the original vessel's resistance of 10.991 N, the combined effect of hull form and trim optimisation yields a total resistance reduction of 7.788%. This cumulative improvement highlights the importance of a holistic design approach that considers both static geometry and dynamic operating trims.

Table 12. Resistance comparison for trim optimisation for optimal hull form.

Cases	Code		LCG (m)	VCG (m)	RT CFD (N)	RT Equation (7) (N)
TR 0	0	0	1.413	0.218	10.735	10.735
TR 9 (Optimal Hull with Optimal Trim)	−2.5	−2.5	1.236	0.191	10.135	9.69
				Difference (%)	−5.589	−9.735
				Difference TR 9 from HF 0 (%)	−7.788	−11.837

The response surface map in Figure 17 exhibits a more complex gradient than the previous scenarios, indicating that the resistance of the optimised hull is highly sensitive to the combined influence of the LCG and VCG. The orientation of the contours suggests that while the LCG remains the dominant factor, the vertical distribution of weight (VCG) now

plays a more prominent role in stabilising the vessel's running trim. The regression model (Equation (7)) predicted a resistance value of 9.69 N, representing a 9.735% reduction. While the CFD result of 10.135 N is slightly more conservative, it validates the model's prediction that the lowest energy state is found at the combined limits of the design variables.

The results of Scenario 3 confirm that the benefits of hull form and trim optimisation are additive. By simultaneously refining the vessel's shape and its hydrostatic balance, a cumulative reduction of nearly 8% in total resistance was achieved. This configuration, designated as TR 9 (Optimal Hull with Optimal Trim), represents the final optimal design proposed in this study. The substantial gain over the initial design justifies the multi-stage optimisation framework as an effective methodology for improving the hydrodynamic performance of the hulls.

3.5.2. Hydrodynamic Characteristics of the Combined Optimal Design

The decomposition of the total resistance into its constituent pressure and shear components for Scenario 3 is presented in Figure 18. This scenario, which represents the integration of the optimised hull geometry and the optimal trim configuration, achieves the most profound reduction in hydrodynamic drag. The CFD results indicate that the pressure resistance was significantly reduced from the baseline of 3.2273 N to 2.6603 N. This decline of approximately 17.5% in the pressure component highlights the effectiveness of combining structural hull refinements with precise weight distribution to mitigate form drag and wave-making energy losses.

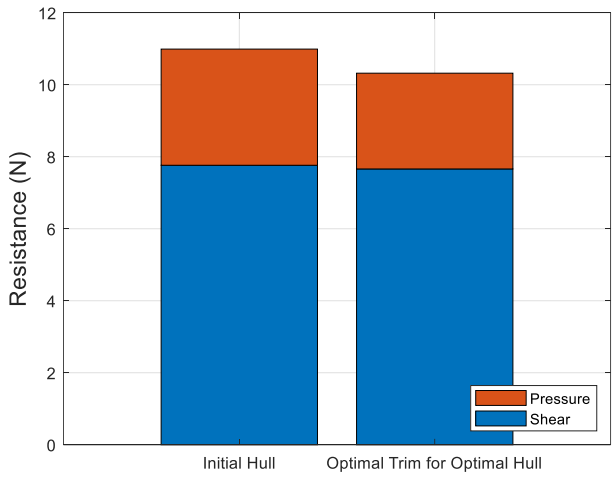


Figure 18. Comparison of resistance for the initial hull (HF 0) and optimal hull with the optimal trim (TR 9). Initial—pressure = 3.2273 N, shear = 7.7633 N; optimal—pressure = 2.6603 N, shear = 7.6614 N.

Furthermore, the shear resistance also exhibited a noticeable improvement, decreasing from 7.7633 N to 7.6614 N. While the magnitude of reduction in the shear component is traditionally smaller in pioneer vessels due to the viscous nature of the water–hull interaction, this decrease suggests that the 'Optimal Hull with Optimal Trim' configuration successfully maintains a more efficient wetted surface area. The cumulative effect of these improvements results in the global minimum of resistance observed in this study. This confirms that the synergy between a refined hull form and a 2.13-degree dynamic trim not only streamlines the pressure field but also optimises the frictional profile, establishing Scenario 3 as the definitive energy-efficient configuration for the vessel.

The optimal trim angles of the initial and optimised hull forms are very similar, with only a small difference observed. Although the longitudinal centre of gravity (LCG) and vertical centre of gravity (VCG) are located differently in the two hull configurations, both

hulls reach nearly the same optimal trim condition. This result indicates that the optimal trim angle of the vessel remains consistent despite the hull form modifications.

As shown in Figure 19, the relationship between the centre of gravity (G), centre of floatation (F), and centre of buoyancy (B) exhibits a similar pattern for both hull forms. The initial hull reaches its optimal condition at a trim angle of approximately 2.23°, while the optimised hull achieves minimum resistance at about 2.13°. This similarity suggests that the equilibrium condition required to obtain minimum resistance is mainly governed by the principal dimensions and displacement of the vessel.

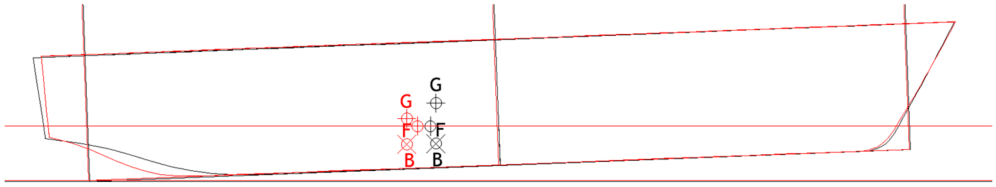


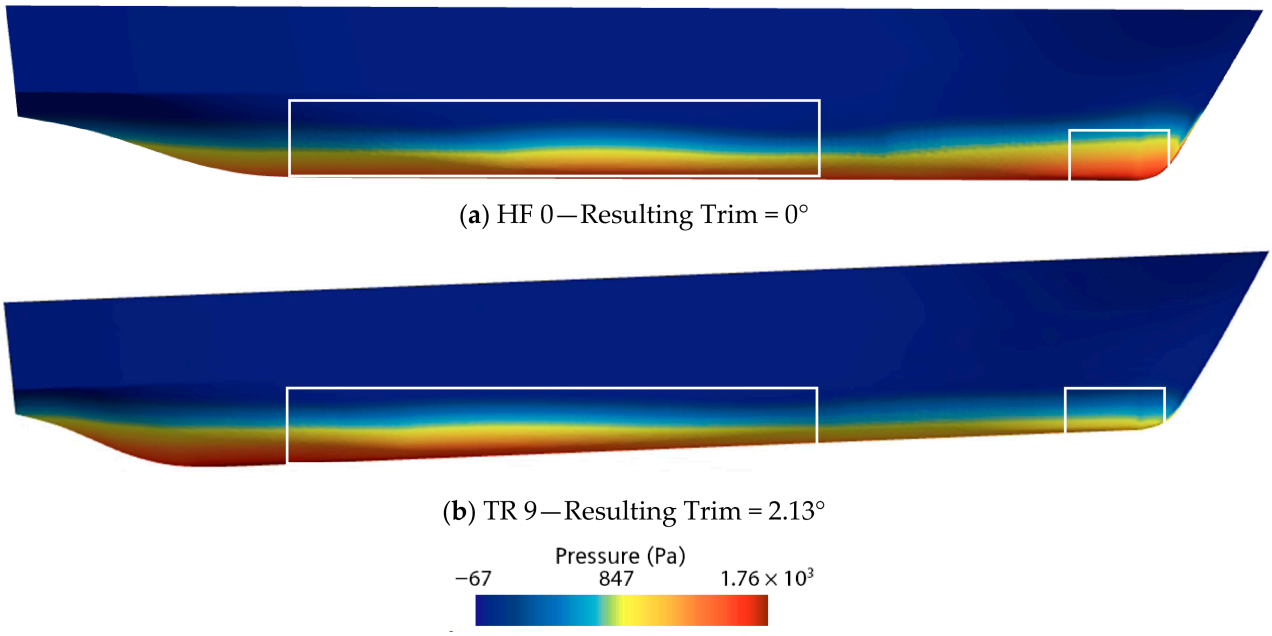
Figure 19. Comparison of the initial hull with optimal trim (LC 9, black line) and the optimal hull with optimal trim (TR 9, red line).

The very small difference in optimal trim angle (approximately 0.1°) shows that the stern trim is an important and stable hydrodynamic characteristic for this type of vessel. This finding is beneficial for ship operators because it indicates that the advantages of trim optimisation remain reliable and are not significantly influenced by small changes in hull geometry or prismatic coefficient.

The visual evidence of the pressure distribution for Scenario 3 reveals the most efficient hydrodynamic state achieved in this study. As shown in Figure 20, the combined application of hull form refinement and optimal trim results in a dramatic transformation of the pressure field compared to the initial vessel. The high-pressure stagnation zone at the bow is significantly reduced in both intensity and area. This physical change corresponds directly to the substantial decrease in pressure resistance, which fell from 3.2273 N to 2.6603 N. By optimising the entry angle and the LCG simultaneously, the vessel minimises the "bulldozing" effect of the bow, allowing for a much smoother pressure recovery along the hull.

A quantitative assessment of the vessel's dynamic trim in this hybrid scenario indicates that the optimal performance is reached at a bow-up trim of approximately 2.13°. In Figure 20, this inclination is clearly visible in the optimal plot, where the deck baseline tilts upward relative to the initial design. This trim, combined with the optimised LCB and Cb of the hull, allows the vessel to achieve a near-perfect hydrodynamic balance. This specific orientation ensures that the most buoyant and streamlined parts of the hull are utilised to pierce the water surface, effectively reducing the form drag and resulting in the study's peak efficiency gain of 7.788% at the design speed.

The analysis of the wave system via the Volume Fraction of Air (VFA) contours further validates the superiority of the Optimal Hull with Optimal Trim configuration. In the initial state, the bow generates a steep, turbulent wave crest that represents significant energy loss. However, the optimal hybrid design produces the flattest wave profile observed across all scenarios. The 2.13-degree trim works in tandem with the modified hull geometry to suppress the bow wave amplitude and eliminate secondary wave interference. This radical smoothing of the free surface deformation is the primary physical reason for the 17.5% reduction in the pressure resistance component, confirming that the vessel is wasting far less energy on wave-making.

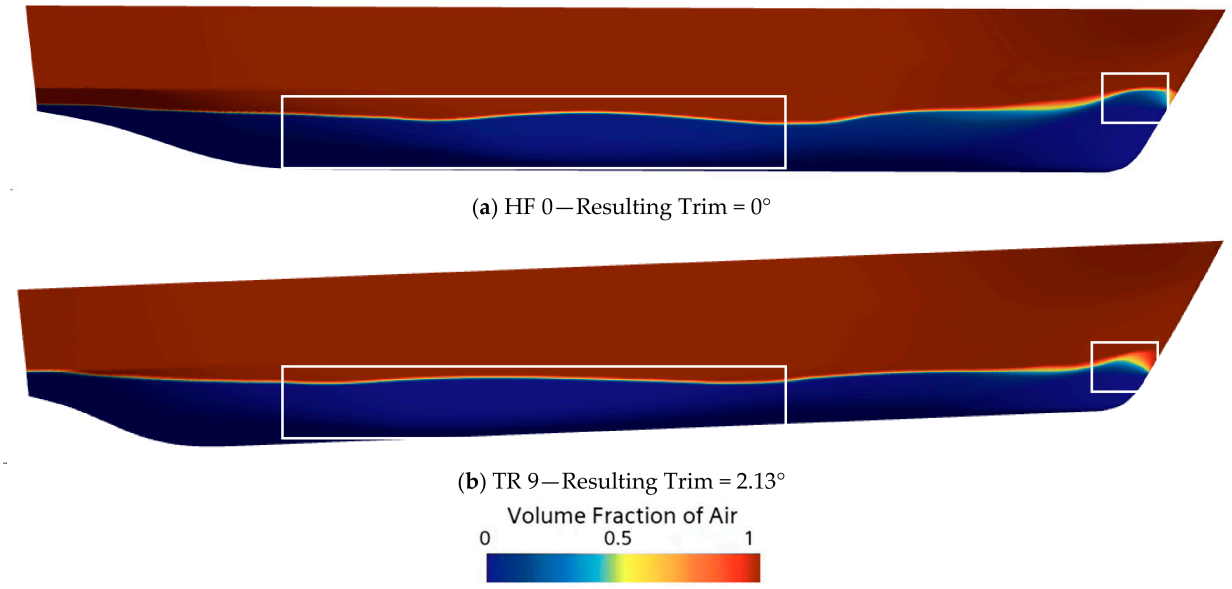


(**a**) HF 0—Resulting Trim = 0°

(**b**) TR 9—Resulting Trim = 2.13°

Figure 20. Pressure distribution of the initial hull form, HF 0 (**a**), and the optimal hull with optimal trim, TR 9 (**b**). The white boxes indicate the specific regions of interest for pressure distribution comparison.

Furthermore, the synergy of this hybrid approach also explains the slight but meaningful reduction in shear resistance down to 7.6614 N. The VFA contours illustrate that the combined optimisation not only improves the wave system but also stabilises the wetted surface area. By maintaining a 2.13-degree trim by the stern, the vessel avoids unnecessarily deep immersion of the hull's midsection, thereby minimising viscous friction. This integrated result, as visualised in Figure 21, provides a comprehensive physical justification for the high R^2 values of the RSM models and demonstrates that the most effective way to optimise pioneer vessels is through a simultaneous consideration of structural geometry and operational trim.



(**a**) HF 0—Resulting Trim = 0°

(**b**) TR 9—Resulting Trim = 2.13°

Figure 21. Free surface contour at the hull with the initial hull form, HF 0 (**a**), and the optimal hull with optimal trim, TR 9 (**b**). The white boxes indicate the specific regions of interest for free surface comparison.

3.6. Comparative Analysis of Optimisation Strategies Across Speed Ranges

The performance of the three optimisation scenarios exhibits distinct characteristics when evaluated across the model speed ranges from 1.455 m/s to 2.061 m/s. As detailed in Table 13 and Figure 22, while all strategies successfully reduce total resistance, their effectiveness varies significantly with the Froude number. In the lower speed range (Fr 0.26 to 0.30), Scenario 2 (Trim Optimisation) frequently outperforms Scenario 1 (Hull Optimisation). For instance, at Fr 0.30, trim adjustments alone achieved a 5.09% reduction compared to the modest 0.83% gained from hull modification. This suggests that for pioneer vessels operating at economical speeds, hydrostatic balance and running trim are more critical factors for efficiency than minor geometric alterations.

Table 13. Comparison of resistance for different scenarios.

V Model (m/s)	Fr (-)	RT (N) Initial	RT (N) Scenario 1	RT (N) Scenario 2	RT (N) Scenario 3
1.455	0.26	10.991	10.735	10.862	10.322
1.576	0.28	14.112	13.830	13.601	13.270
1.698	0.30	18.358	18.205	17.423	17.263
1.819	0.32	22.617	22.369	21.742	21.336
1.94	0.34	27.716	26.418	26.686	25.705
2.061	0.36	35.554	32.464	33.636	32.286

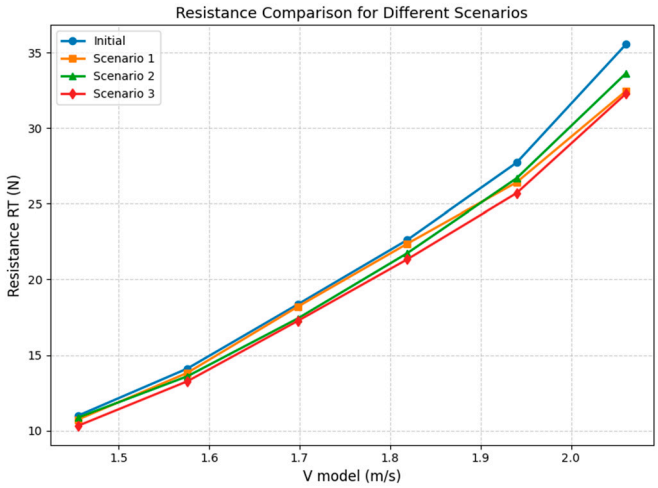


Figure 22. Comparison of resistance for different scenarios.

However, as the vessel speed increases towards the design limit of Fr 0.36, the impact of hull form optimisation becomes more pronounced. In Table 14, the resistance reduction in Scenario 1 jumps from 1.097% at Fr 0.32 to a substantial 8.69% at Fr 0.36. This trend indicates that the refined hull geometry is specifically optimised to mitigate wave-making resistance, which dominates the total resistance profile at higher velocities. In contrast, the benefits of trim optimisation in Scenario 2 appear to stabilise or even slightly diminish in relative terms at peak speeds, highlighting the physical limitations of weight distribution when the hull form itself is not hydrodynamically ideal for high-speed flow.

Table 14. Total resistance reduction for different scenarios.

V Model (m/s)	Fr	Scenario 1 vs. Initial	Scenario 2 vs. Initial	Scenario 3 vs. Initial
1.455	0.26	−2.329	−1.174	−6.087
1.576	0.28	−1.998	−3.621	−5.967
1.698	0.30	−0.833	−5.093	−5.965
1.819	0.32	−1.097	−3.869	−5.664
1.94	0.34	−4.683	−3.716	−7.256
2.061	0.36	−8.691	−5.395	−9.192

The most compelling results are found in Scenario 3, which demonstrates a superior and consistent performance across the entire speed spectrum. By combining hull refinement with optimal trim, this "hybrid" strategy achieves a resistance reduction of approximately 6% at lower speeds and reaches a peak efficiency gain of 9.19% at Fr 0.36. Unlike the other scenarios, Scenario 3 effectively bridges the gap between low-speed hydrostatic efficiency and high-speed hydrodynamic performance. For ship designers and operators, these findings recommend a tiered implementation: trim optimisation should be prioritised for immediate operational energy savings in existing fleets, while a combined hull–trim integrated design remains the definitive standard for new-build pioneer vessels seeking maximum fuel economy. This result shows that this optimisation can reduce the resistance at multiple speeds, as shown in Table 14. This optimisation process benefits designers by reduced optimisation time by not including multiple speeds, as observed in [14].

Figure 23 shows a comprehensive breakdown of resistance components, derived from the systematic CFD simulations across the speed variations (1.455 m/s to 2.061 m/s). It highlights a clear shift in the hydrodynamic profile of the pioneer vessel. At lower speeds, such as Vs = 1.455 m/s, the total resistance is dominated by shear forces, with the initial hull exhibiting a shear resistance of 7.7633 N compared to a pressure resistance of 3.2273 N. In this regime, the 'Initial Hull with Optimal Trim' (Scenario 2) demonstrates a superior ability to reduce pressure resistance (3.1132 N) compared to the geometric changes in Scenario 1 (3.0189 N). This trend confirms that at low Froude numbers, the vessel's efficiency is more sensitive to its hydrostatic orientation and trim-induced pressure recovery than to minor modifications in hull geometry.

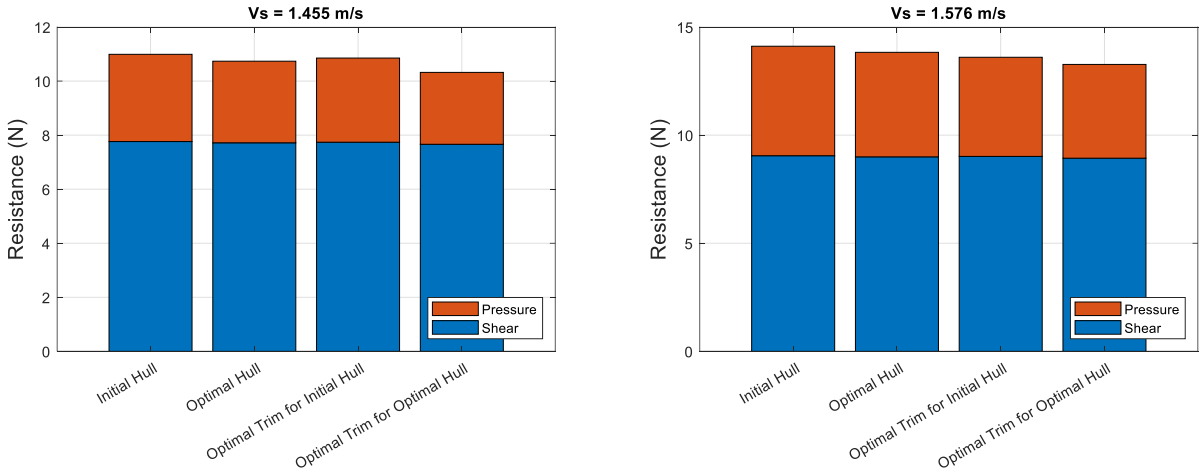


Figure 23. *Cont.*

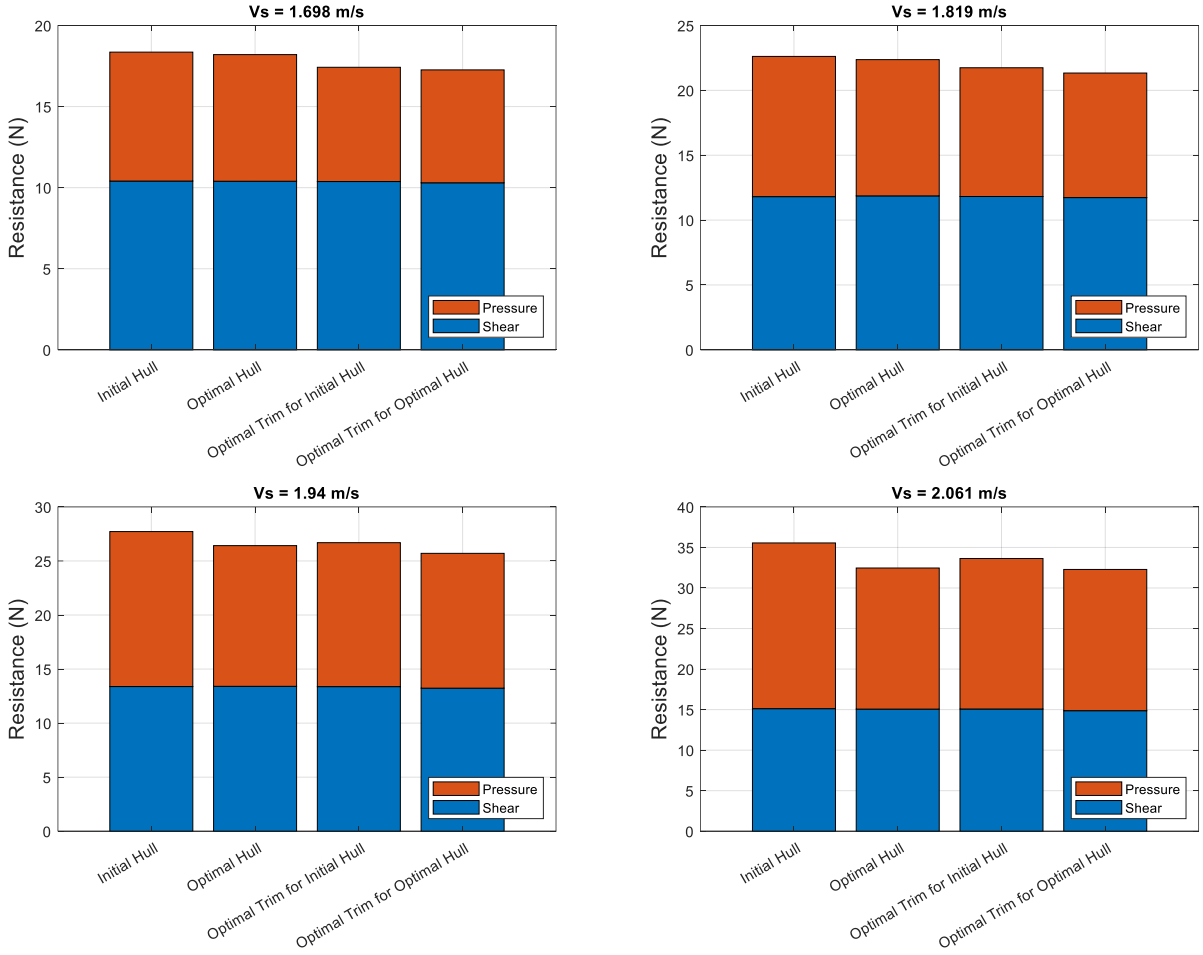


Figure 23. The components of total resistance for different scenarios at specific speeds.

However, as the velocity increases to the maximum design speed of Vm = 2.061 m/s, the pressure resistance becomes the dominant component, soaring to 20.4365 N for the initial hull, while shear resistance reaches 15.1176 N. In this high-speed regime, the effectiveness of the 'Optimal Hull' (Scenario 1) becomes significantly more pronounced, reducing pressure resistance to 17.4009 N. The most improvement is consistently achieved by the Optimal Hull with Optimal Trim (Scenario 3), which yields a pressure resistance of 17.4195 N and a shear resistance of 14.8668 N at peak speed. This integrated approach ensures that the vessel maintains a global minimum of resistance by simultaneously suppressing wave-making energy at high speeds and optimising the frictional profile, thereby validating Scenario 3 as the most resilient configuration across the entire operational envelope.

3.7. Practical Implications and Design Recommendations

The findings of this study offer significant strategic value for the development and operational management of pioneer vessels, particularly within the context of the maritime industry's lifecycle. For new building projects, the results from Scenario 1 underscore the critical importance of initial hull form optimisation. By refining geometric parameters such as LCB and Cb during the preliminary design stage, a permanent reduction in resistance is locked in for the vessel's entire service life, typically spanning 20 to 25 years. The data demonstrates that this structural optimisation is particularly potent at higher speeds, achieving a significant 8.69% reduction in resistance at Fr 0.36, which translates directly into long-term fuel savings and a reduced carbon footprint.

For the existing fleet of pioneer vessels already in service, where structural modifications are often cost-prohibitive, Scenario 2 provides a compelling "low-cost" alternative through operational trim optimisation. Since operators cannot easily alter the physical hull form, adjusting the longitudinal and vertical centres of gravity (LCG and VCG) through strategic cargo distribution or ballast management offers a viable pathway to efficiency. The analysis shows that such adjustments can mitigate resistance by up to 5.39% at peak speeds without requiring any capital expenditure for construction, making it an ideal strategy for immediate energy efficiency improvements in active fleets.

This study further highlights that maximum hydrodynamic efficiency is achieved through a hybrid strategy, as evidenced by the superior performance of Scenario 3. The results suggest that focusing on either hull geometry or trim in isolation is insufficient for reaching the global minimum resistance. Scenario 3, which combines a refined hull with an optimal trim configuration, yields the most consistent and robust performance across the entire speed range. Notably, this combined approach provides significantly higher stability in resistance reduction at lower speeds (Fr 0.26) compared to Scenario 1 alone, ensuring that the vessel operates efficiently even outside its primary design speed.

Consequently, it is strongly recommended that naval architects and ship designers incorporate operational trim considerations as early as possible in the hull design phase. By anticipating the vessel's running trim and integrating it into the CFD-based optimisation process, a more resilient design can be produced. This proactive integration ensures that the vessel remains efficient under varying load conditions, a characteristic that is particularly beneficial for pioneer vessels that often face fluctuating cargo volumes during their service in remote regions.

To evaluate the practical application of the optimisation results, two distinct implementation strategies are proposed. Scenario 2 is categorised as an operational-based solution suitable for existing vessels, where the target trim is achieved through internal weight management (e.g., ballast water adjustment or cargo longitudinal positioning) without requiring structural changes.

In Scenario 3, the vessel is designed with a slanted keel (raked keel) to achieve the optimal hydrodynamic trim. To ensure operational safety, the main deck is constructed with a longitudinal slope relative to the baseline, effectively creating a level working platform when the ship is at its design trim of 2.13°. This configuration, often referred to in newbuild designs as an integrated deck-to-trim adjustment, allows for the benefits of reduced resistance without the safety risks associated with an inclined floor.

As illustrated in Figure 24, by adjusting the main deck geometry to counteract the longitudinal tilt, the working platform remains perfectly level during operation while the hull maintains its hydrodynamically superior trim attitude. This design integration ensures that the resistance reduction is achieved without the practical drawbacks of a permanent deck inclination, thereby facilitating safer cargo handling and improved onboard comfort for vessels operating in the challenging conditions of the Indonesian archipelago.

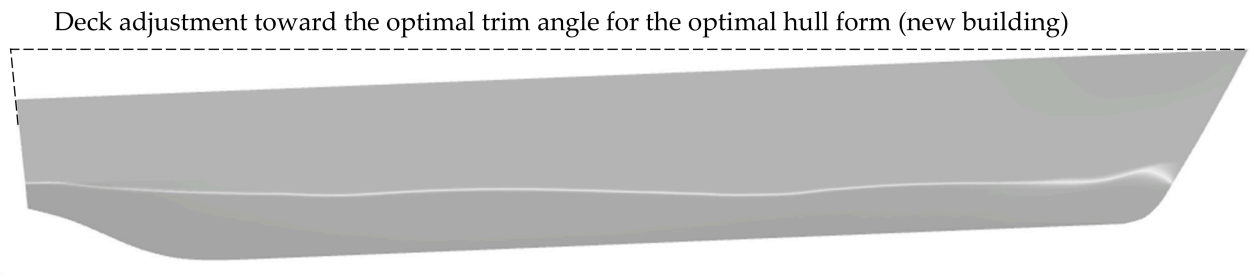


Figure 24. Recommendation for deck adjustment toward the optimal trim angle for the optimal hull form.

The sensitivity analysis regarding operational speed also provides vital insights for daily fleet management. Data from Tables 13 and 14 reveal that at lower, more economical speeds (12 to 14 knots at full scale), Scenario 2 (trim optimisation) is occasionally more effective than Scenario 1 (hull optimisation). For instance, at 14 knots, trim adjustments achieved a 5.09% reduction, whereas hull modifications only yielded a 0.83% reduction. This indicates that for vessels frequently operating at lower speeds to conserve fuel, precise trim management is not merely a secondary adjustment but the primary driver of daily fuel economy.

These implications suggest a tiered approach to maritime energy management. For the design of future pioneer vessels, a combined hull-trim optimisation framework should be adopted to achieve peak performance, as seen in the 9.19% maximum reduction in Scenario 3. Simultaneously, for existing ships, the implementation of an optimal trim should be prioritised. Such strategies are essential for the Indonesian maritime sector to meet stringent international environmental standards (EEDI/EEXI) while maintaining the economic viability of vital transport routes in remote archipelagic areas.

4. Conclusions

This study has successfully implemented a multi-scenario optimisation framework to enhance the hydrodynamic performance of a pioneer vessel using a combination of Computational Fluid Dynamics (CFD) and the Central Composite Design (CCD) variant of the Response Surface Methodology (RSM). The numerical model was rigorously validated against experimental data, yielding a remarkably low mean absolute percentage error (MAPE) of 1.545%, while the grid convergence study confirmed a high level of numerical certainty with a GCI of 0.3472%. These results establish a robust foundation for the subsequent optimisation phases.

The statistical analysis through RSM proved highly effective, with all three regression models achieving R^2 values exceeding 0.994. Scenario 3, which combined hull form and trim optimisation, emerged as the most statistically superior model, providing the lowest standard error (0.0263) and the highest predictive accuracy. The Analysis of Variance (ANOVA) further confirmed the significance of the models, with *p*-values consistently below the 0.05 threshold, validating that the relationship between the design variables (LCB, Cb, and trim parameters) and vessel resistance was captured with high fidelity.

The optimisation results reveal significant hydrodynamic improvements across all investigated scenarios:

- Scenario 1 (Hull Optimisation) achieved a maximum resistance reduction of 8.691% at Fr 0.36 by refining the LCB and Cb.
- Scenario 2 (Trim Optimisation for Initial Hull) demonstrated that active weight distribution alone could reduce resistance by up to 5.395% at peak speeds.
- Scenario 3 (Combined Hybrid Optimisation) yielded the best overall performance, achieving a total resistance reduction of 9.192% at peak speeds.

Crucially, the study highlights a speed-dependent sensitivity: while hull form modification is more effective at higher speeds, trim optimisation offers superior efficiency gains at lower, more economical speeds (12–14 knots in full scale). These findings lead to the conclusion that for pioneer vessels, a hybrid approach, integrating an optimal hull design with optimal trim, is essential for achieving maximum fuel efficiency and regulatory compliance. This research provides a clear roadmap for ship designers and operators to implement tiered energy-saving strategies for both new-build projects and existing fleet operations in the archipelagic context.

Author Contributions: Conceptualization, M.I.; Methodology, M.I. and A.T.; Software, A.N.A.R. and A.M.W.; Validation, A.N.A.R. and A.M.W.; Formal analysis, A.N.A.R. and A.M.W.; Investigation, M.I.; Resources, A.T., B.A.A. and A.F.; Data curation, A.F.; Writing—original draft, M.I., A.T., B.A.A. and A.F.; Writing—review & editing, M.I., A.T., B.A.A. and A.F.; Supervision, M.I. and B.A.A.; Project administration, M.I. All authors have read and agreed to the published version of the manuscript.

Funding: This research was funded by Universitas Diponegoro with contract number: 222-592/UN7.D2/PP/IV/2025.

Institutional Review Board Statement: Not applicable.

Informed Consent Statement: Not applicable.

Data Availability Statement: Dataset available on request from the authors.

Acknowledgments: The authors would like to express their gratitude to Universitas Diponegoro for funding this research through the International Publication Research (RPI) scheme, under the non-state budget (*Selain APBN*) for the 2025 fiscal year (Contract No: 222-592/UN7.D2/PP/IV/2025).

Conflicts of Interest: The authors declare no conflict of interest.

References

1. Gusti, A.P.; Semin Dinariyana, A.A.B.; Irawan, M.I.; Furusho, M. Reduction in ship fuel consumption and emission by sailing at slow speeds. *J. Eng. Sci. Technol.* **2019**, *14*, 3267–3281.
2. Feng, Y.; el Moctar, O.; Jiang, C. Hydrodynamic optimization of containership design to minimize wave-making and wave-added resistance using a weak-scatterer approach. *Phys. Fluids* **2025**, *37*, 027146. [CrossRef]
3. Iqbal, M.; Terziev, M.; Tezdogan, T.; Incecik, A. Hull form optimisation to minimise the total resistance and dynamic responses of small fishing vessels. *Ocean Eng.* **2025**, *321*, 120357. [CrossRef]
4. Song, S.; Zhang, B. Trim Optimization Evaluation and Design of a Container Ship. In *Proceedings of the Advances in Machinery, Materials Science and Engineering Application X: Proceedings of the 10th International Conference (MMSE 2024), Paris, France, 27–28 July 2024*; IOS Press: Amsterdam, The Netherlands, 2024; pp. 841–846.
5. Kim, Y.; Ozyurt, R. Underestimated penalty of hull fouling: A scenario-based analysis of GHG emissions from global shipping. *Appl. Ocean Res.* **2025**, *165*, 104870. [CrossRef]
6. Tian, X.; Xie, T.; Liu, Z.; Lai, X.; Pan, H.; Wang, C.; Leng, J.; Rahman, M.M. Study on the resistance of a large pure car truck carrier with bulbous bow and transom stern. *J. Mar. Sci. Eng.* **2023**, *11*, 1932. [CrossRef]
7. Sun, H.; Faltinsen, O.M. Hydrodynamic forces on a semi-displacement ship at high speed. *Appl. Ocean Res.* **2012**, *34*, 68–77. [CrossRef]
8. Çelik, C.; Danışman, D.B. Powering performance prediction of a semi-displacement ship retrofitted with Hull Vane. *Ocean Eng.* **2023**, *286*, 115561. [CrossRef]
9. Krishnan, G.; Vijayakumar, R.; Milanov, E.; el Moctar, O. Analysis of the impact of air lubrication on the hydrodynamic performance of KVLCC2. *Ocean Eng.* **2026**, *344*, 123513. [CrossRef]
10. Park, S.H.; Lee, I. Optimization of drag reduction effect of air lubrication for a tanker model. *Int. J. Nav. Archit. Ocean Eng.* **2018**, *10*, 427–438. [CrossRef]
11. Zhang, H.; Wei, Y.; Xiao, S.; Zhao, Z. Ship hull resistance minimization using surrogate modelling and an improved dung beetle optimizer. *Ocean Eng.* **2025**, *322*, 120588. [CrossRef]
12. Ngoc, V.M.; Ha, N.T.H.; Ngoc, P.M.; Van Tung, D.; Hao, N.H.; Tu, T.N. Numerical Investigation on the Influence of Ship Hull Form Modification on Resistance of the 4600DWT Cargo Ship Using RANSE Method. *IOP Conf. Ser. Earth Environ. Sci.* **2023**, *1278*, 12023. [CrossRef]
13. Iqbal, M.; Samuel, S. Traditional catamaran hull form configurations that reduce total resistance. *Int. J. Technol.* **2017**, *8*, 85–93. [CrossRef]
14. Liu, J.; Zhang, B.; Hu, L.; Bi, J.; Tian, Z.; Dong, Y. Research on hull form optimization at multiple speeds based on machine learning and ship model experiments. *Eng. Appl. Artif. Intell.* **2025**, *160*, 111882. [CrossRef]
15. Mahmoodi, H.; Hajivand, A. Numerical trim and draft optimization of a twin-screw modern surface combatant with inverted bow. *Appl. Ocean Res.* **2022**, *123*, 103186. [CrossRef]
16. Reichel, M.; Minchev, A.; Larsen, N.L. Trim optimisation-theory and practice. *TransNav Int. J. Mar. Navig. Saf. Sea Transp.* **2014**, *8*, 387–392. [CrossRef]
17. Hüffmeier, J.; Lundman, J.; Elern, F. *Trim and Ballast Optimization for a Tnaker Based on Machine Learning*; Ecoprodigi, Intereg Baltic Sea Region: Gothenburg, Sweden, 2020.

18. Duan, W.; Zhang, H.; Huang, L.; Liu, J.; Shao, W.; Cao, G.; Shi, Z. Numerical simulation of trim optimization on resistance performance based on CFD method. In *Proceedings of the International Conference on Offshore Mechanics and Arctic Engineering, Glasgow, UK, 9–14 June 2019*; American Society of Mechanical Engineers: New York, NY, USA, 2019; p. V002T08A051.
19. Shivachev, E.; Khorasanchi, M.; Day, S.; Turan, O. Impact of trim on added resistance of KRISO container ship (KCS) in head waves: An experimental and numerical study. *Ocean Eng.* **2020**, *211*, 107594. [CrossRef]
20. Wen, P.; Fadillah, A. The Effect of Trim on Stability and Seakeeping of Tanker, Container, and Bulk Carrier. *IOP Conf. Ser. Earth Environ. Sci.* **2022**, *972*, 12037. [CrossRef]
21. Lee, S.-S.; Lee, J.-C.; Shin, S.-C.; Kim, S.-Y.; Yoon, H.-S. A study on optimization of ship hull form based on neuro-response surface method (NRSM). *J. Mar. Sci. Technol.-Taiwan* **2014**, *22*, 12.
22. Arai, M.; Shimizu, T. Optimization of the design of ship structures using response surface methodology. In *Practical Design of Ships and Other Floating Structures*; Elsevier: Amsterdam, The Netherlands, 2001; pp. 331–339.
23. Coppedè, A.; Gaggero, S.; Vernengo, G.; Villa, D. Hydrodynamic shape optimization by high fidelity CFD solver and Gaussian process based response surface method. *Appl. Ocean Res.* **2019**, *90*, 101841. [CrossRef]
24. Iqbal, M.; Trimulyono, A.; Samuel; Mursid, O. Study of applicability in minimising pitch radius gyration for different hull types to improve seakeeping performance. *J. Mar. Sci. Eng.* **2025**, *13*, 1734. [CrossRef]
25. Lackenby, H. On the systematic geometrical variation of ship forms. *Trans. R. Inst. Nav. Archit.* **1950**, *92*, 289–316.
26. Kramer, M.E. Automating Lackenby's Method: The Design of a Set of Scripts to Execute Lackenby's Method with McNaull's Expansion in Rhinoceros 3D. Master's Thesis, The University of New Orleans, New Orleans, LA, USA, 2023.
27. Terziev, M.; Tezdogan, T.; Incecik, A. Scale effects and full-scale ship hydrodynamics: A review. *Ocean Eng.* **2022**, *245*, 110496. [CrossRef]
28. ITTC. Practical Guidelines for Ship Resistance CFD. 2014. Available online: https://www.ittc.info/media/9775/75-03-02-04.pdf (accessed on 9 April 2026).
29. Richardson, L.F., IX. The approximate arithmetical solution by finite differences of physical problems involving differential equations, with an application to the stresses in a masonry dam. *Philos. Trans. R. Soc. Lond. Ser. A Contain. Pap. A Math. Phys. Character* **1911**, *210*, 307–357. [CrossRef]
30. Celik, I.B.; Ghia, U.; Roache, P.J.; Freitas, C.J. Procedure for Estimation and Reporting of Uncertainty Due to Discretization in CFD Applications. *J. Fluids Eng.* **2008**, *130*, 078001. [CrossRef]
31. Burmester, S.; Vaz, G.; el Moctar, O. Towards credible CFD simulations for floating offshore wind turbines. *Ocean Eng.* **2020**, *209*, 107237. [CrossRef]

Disclaimer/Publisher's Note: The statements, opinions and data contained in all publications are solely those of the individual author(s) and contributor(s) and not of MDPI and/or the editor(s). MDPI and/or the editor(s) disclaim responsibility for any injury to people or property resulting from any ideas, methods, instructions or products referred to in the content.